minerals

MDPI

Article

Integration of Whole-Rock Geochemistry and Mineral Chemistry Data for the Petrogenesis of A-Type Ring Complex from Gebel El Bakriyah Area, Egypt

Ahmed A. Abd El-Fatah [1,*], Adel A. Surour [1,2], Mokhles K. Azer [3] and Ahmed A. Madani [1]

[1] Department of Geology, Faculty of Science, Cairo University, Giza 12613, Egypt; adelsurour@cu.edu.eg (A.A.S.); aamadani@sci.cu.edu.eg (A.A.M.)
[2] Department of Geological Sciences, Faculty of Science, Galala University, New Galala City 43511, Egypt
[3] Geological Sciences Department, National Research Centre, Giza 12622, Egypt; mk.abdel-malak@nrc.sci.eg
* Correspondence: aabdeldayiem@sci.cu.edu.eg

Abstract: El Bakriyah Ring Complex (BRC) is a prominent Neoproterozoic post-collisional granite suite in the southern part of the Central Eastern Desert of Egypt. The BRC bears critical materials (F, B, Nb, and Ta) in appreciable amounts either in the form of rare-metals dissemination or in the form of fluorite and barite vein mineralization. The complex consists of inner syenogranite and outer alkali feldspar granite that have been emplaced in a Pan-African assemblage made up of granitic country rocks (granodiorite and monzogranite), in addition to post-collisional fresh gabbro as a part of the Arabian-Nubian Shield (ANS) in northeast Africa. Granites of the BRC are characterized by enrichment in silica, alkalis, Rb, Y, Ga, Nb, Ta, Th, and U and depletion in Sr, Ba, and Ti. Geochemical characterization of the BRC indicates that the magma is a crustal melt, which originated from the partial melting of metasedimentary sources. Concentrations of rare-earth elements (REEs) differ in magnitude from the ring complex and its granitic country rocks but they have similar patterns, which are sub-parallel and show LREEs enrichment compared to HREEs. The presence of a negative Eu anomaly in these rocks is related to plagioclase fractionation. The abundance of fluorine (F) in the different granite varieties plays an important role in the existence of a tetrad influence on the behavior of REEs (TE1, 3 = up to 1.15). Geochemical parameters suggest the crystallization of the BRC granite varieties by fractional crystallization and limited assimilation. Mn-columbite and Mn-tantalite are the most abundant rare-metals dissemination in the BRC granite varieties. We present combined field, mineralogical and geochemical data that are in favor of magma originating from a metasedimentary source for the BRC with typical characteristics of A-type granites. Our geodynamic model suggests that the Gebel El Bakriyah area witnessed the Neoproterozoic post-collisional stage of the ANS during its late phase of formation. This stage was characterized by the emplacement of fresh gabbros followed by the syenogranite and alkali-feldspar granite of the BRC into an arc-related assemblage (granodiorite and monzogranite). It is believed that the mantle-derived magma was interplated and then moved upward in the extensional environment to a shallower level in the crust owing to events of lithospheric delamination. This presumably accelerated the processes of partial melting and differentiation of the metasedimentary dominated source (Tonian-Cryogenian) to produce the A-type granites building up the BRC (Ediacaran).

Keywords: El Bakriyah ring complex; A-type granites; fractional crystallization; metasedimentary source; Ediacaran post-collisional magmatism

Citation: Abd El-Fatah, A.A.; Surour, A.A.; Azer, M.K.; Madani, A.A. Integration of Whole-Rock Geochemistry and Mineral Chemistry Data for the Petrogenesis of A-Type Ring Complex from Gebel El Bakriyah Area, Egypt. *Minerals* **2023**, *13*, 1273. https://doi.org/10.3390/min13101273

Academic Editors: Ignez de Pinho Guimarães and Jefferson Valdemiro De Lima

Received: 23 August 2023
Revised: 23 September 2023
Accepted: 27 September 2023
Published: 29 September 2023

1. Introduction

The Eastern Desert of Egypt, as a part of the Neoproterozoic Arabian-Nubian Shield (ANS), is occupied by voluminous masses of granitic rocks that formed from different melt compositions and emplaced in different tectonic regimes (e.g., [1–3]). In the Gebel El Bakriyah area, which is located in the central part of the Eastern Desert (CED), prominent

granitic masses are present that have field and laboratory characteristics, which can be integrated with other rock units such as gabbros to build up a geodynamic model for better understanding of the ANS evolution. The term "granitic rocks" is used here to denote two contrasting rock types with diversity in mineral composition, chemical composition, and tectonic setting. They include "proper granites" and "granitoids" such as quartz-diorite, granodiorite, and tonalite. They together constitute about 60% of plutonic rocks of the Nubian Shield in the Eastern Desert and can be classified and distinguished according to mineral and chemical compositions, magma type, tectonic setting, and age (e.g., [2,4,5]). In a recent review, [3] classified the Egyptian granitic rocks (mainly in the Eastern Desert and the Sinai Peninsula) based on the tectonic regime into four types namely, subduction-related, collisional, calc-alkaline post-orogenic, and alkaline post-tectonic. The subduction-related category (around 700–660 Ma, [6]) is represented by granitoids that are tholeiitic to calc-alkaline and is categorized as the older granitoids [6]. On the other hand, collision-related granites (around 610–590 Ma, [7]) are medium- to high-K calc-alkaline and are represented by younger granites (monzo- to syenogranite) that have been formed by the lower continental crust melting (e.g., [6,8]. Calc-alkaline post-orogenic granite (between 590 and 540 Ma, [3]) is characterized by a high-K calc-alkaline to shoshonite nature and comprises A_2-type younger granites, which originated from a melting process of lower crustal rocks in an extension setting during the transitional stage between orogenic and anorogenic regimes (e.g., [6,9]). The last phase of younger granites (A_1-type) (around 540 Ma, [7]) is the alkaline post-tectonic granite formed by the differentiation of alkali-basaltic magmas (e.g., [9]).

Globally, A-type granites are classified into anorogenic and post-orogenic granites [10], and they represent the youngest phase of felsic magmatism in the Eastern Desert of Egypt and the entire ANS [2,3,11]. For the last three decades, A-type granites in the Eastern Desert attracted considerable attention because of their economic potentialities and occasional enrichment of rare metals (e.g., Nb, Ta, Sn, W, Be, and B), rare-earth elements (REEs) and radioactive materials [4,12]. For example, [13] reported that these mineralizations are in intimate association with accessory minerals like beryl, columbite, tantalite, fergusonite, thorite, cassiterite, wolframite, and monazite. In comparison with I-type granites, A-type granites are deficient in Sr, Ba, Eu, Ca, and large ion lithophile elements (LILE) with abundance in silica, K, Rb, Y, REEs, Zr, and high-field strength elements (HFSE) [14].

A-type granites show vast geographic distribution in the Eastern Desert and extend in age from 630 Ma to 550 Ma [12]. From the petrological point of view, it is believed that these granites have been developed by partial melting of a variety of pre-existing crustal protoliths or by fractionation of mantle-derived mafic magmas (e.g., [15,16]). In the context of our present study, we investigate the Gebel El-Bakriyah younger granite pluton in the central Eastern Desert (CED) of Egypt to have a detailed and comprehensive account of the petrogenetic processes leading to the formation of this prominent A-type granite ring complex. Previously, country rocks of the El Bakriyah Ring Complex (BRC) were investigated by [17,18], whereas additional information about the ring complex is lacking. Therefore, we integrate field and laboratory studies to build up a reasonable geotectonic model in terms of the geodynamic evolution with respect to the main phases of magmatism and tectonism in the northwestern part of the ANS in the CED. Also, we aim to focus on possible rare-metal enrichment in the BRC, which was known in the past for its fluorite and barite mineralizations [19]. We use combined whole-rock geochemistry and mineral chemistry data for mineral characterization and emphasizing magma source and tectonic setting.

2. Geological Setting and Field Observation

The evolution of the basement rocks in the ANS during the Neoproterozoic rocks (850–590 Ma) involved three major stages: (1) pre-collisional, (2) collisional, and (3) post-collisional [2,3]. Ophiolites and metamorphosed volcano-sedimentary successions were formed during the pre-collisional stage (850–700 Ma). The collisional stage (670–630 Ma)

witnessed the emplacement of calc-alkaline magmatic rocks represented by arc-related gabbros and granitoids and their volcanics. The BRC in the CED, which is the main target of the present study, belongs to the third stage (the post-collisional) that is characterized by alkaline magmatism including A-type granites [20,21]. Felsic and mafic magmatism in the CED are abundant and include fresh gabbros side by side with the A-type granites [22]. Association of fresh gabbro and granite is known in the Gebel El Bakriyah area (Figure 1b) and other localities in the CED, e.g., at Wadi El-Faliq and Gebel Atud area e.g., [23,24]. In addition, the CED has post-collisional felsic intrusions at Abu Dabab, Wadi El-Igla, Gebel Mueilha, Homret Waggat, Gebel El-Ineigi e.g., [9,12,13].

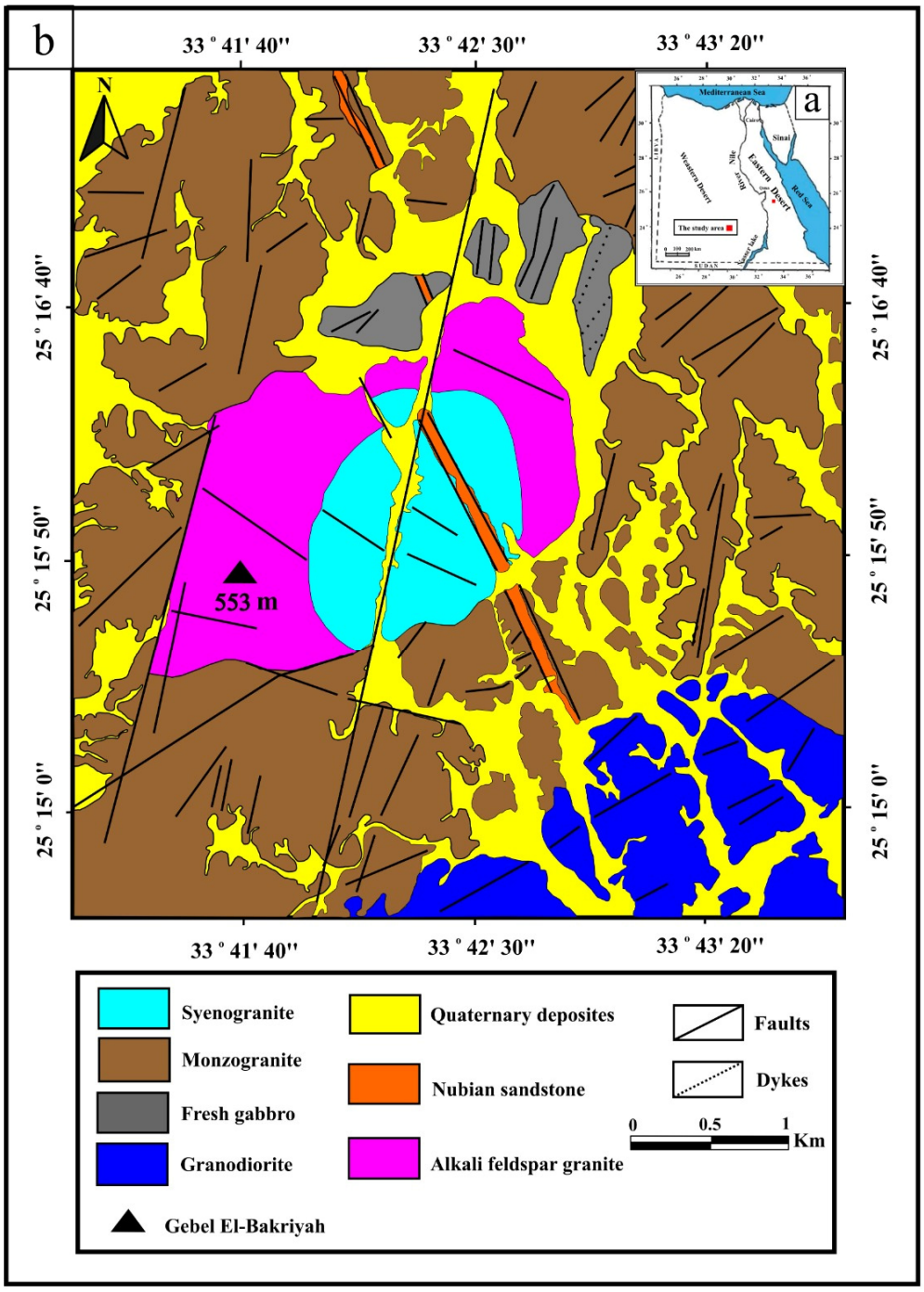

Figure 1. (**a**) Location map of the study area. (**b**) Geological map of the Gebel El Bakriyah area was recently constructed by the present authors [25].

Gebel El Bakriyah area (Figure 1a,b) is located about 15 km north of the El-Barramiya gold mine near the Idfu-Marsa Alam asphaltic road that connects the Red Sea with the Nile Valley. The area is bound by longitudes from 33°41′ to 33°43′ E and by latitudes from 25°15′ to 25°17′ N (Figure 1a,b). In general, the area is characterized by moderate relief, and the only exceptional peak is El Bakriyah Mountain, which has an altitude of ~550 m above the mean sea level. According to [16], Precambrian lithologies in the Gebel El Bakriyah area comprise two main granitic rock types: (1) older granitoids (diorite-granodiorite), and (2) younger granites, mostly syenogranite and much lesser granodiorite. All of them have been emplaced in folded and metamorphosed sequences of metagabbros (Figure 1b). Recently, [23] investigated the fresh post-collisional gabbros and distinguished them into three varieties represented by troctolite, olivine gabbro, and altered hornblende gabbro. Ref. Abd El-Fatah et al. [25] used the remote sensing technique to construct a new geological map of the Gebel El-Bakriyah area (Figure 1b). Using the processed satellite images, it was possible to confirm the rock units and varieties that have been identified in the field and assorted on a mineralogical/petrographical basis. Chronologically, the rocks are arranged from oldest to youngest as follows: granodiorite, fresh gabbro, monzogranite, the BRC (syenogranite and alkali feldspar granite), Nubian sandstone and Quaternary deposits [17,18]. The area is dissected by faults of different ages and types trending N-S, NW-SE, and NE-SW [17]. The only available age (520–506 Ma) for the complex was presented by [26] based on Rb-Sr isochron. In the field, it is easy to distinguish lithological contacts between the core of the BRC (syenogranite) from its rim, which is made up of alkali feldspar granite (Figure 2a). In some instances, and due to intense faulting, contact between the two granite varieties of the BRC is distinctly sharp, i.e., structural. Alkali feldspar granite (Figure 2b) is yellowish to reddish pink in color, coarse- to medium grained and among its outcrops is the summit of El Bakriyah Mountain, and is traversed by quartz, barite, and fluorite veins (Figure 2c,d). The syenogranite is pale pink to red, medium-grained, and displays sharp contact with the Nubian sandstone. Country rocks for the BRC are mostly monzogranite, which forms moderately elevated hills, pink in color, and coarse- to medium-grained. This monzogranite is hard, massive, and dissected by two different sets of joints, and displays sharp contact with the BRC. In the southern part of the Gebel El Bakriyah area, there is some localized grey granodiorite, which forms low relief topography intruded by monzogranite (Figure 2e). There are occasional xenoliths of monzogranite in some granodiorite outcrops. Fresh gabbro forms sporadic outcrops, which constitute four masses located nearly in the central part and northeast extreme of the area (Figure 1b). The gabbro varieties are hard, coarse-grained, and show no layering. The hornblende gabbro variety shows the highest degree of weathering and alterations compared with troctolite and olivine gabbro. In some instances, troctolite is invaded by NE-SW trending mafic and felsic dykes. The Nubian sandstone, of a Late Cretaceous age, non-conformably caps the Precambrian basement rocks.

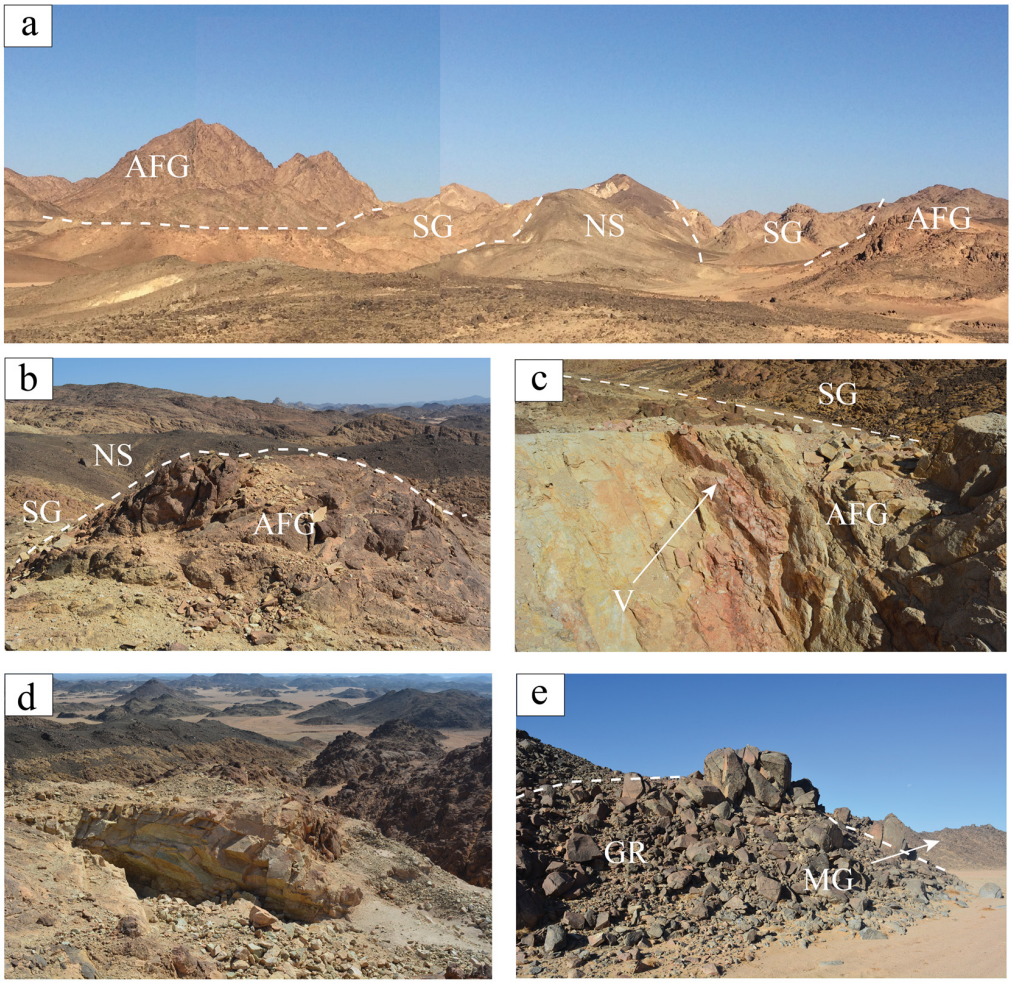

Figure 2. Geologic setup and field relationships. (**a**) General view of the granite varieties forming the El Bakriyah ring complex (BRC); namely syenogranite core (SG) and alkali feldspar granite rim (AFG) non-conformably capped by the Nubian sandstone (NS). (**b**) The rugged peak of alkali feldspar granite (AFG) capped by Nubian sandstone (NS) and juxtaposing syenogranite (SG). (**c**) Mineralized fluorite vein (V), with some barite, cross-cutting the alkali feldspar granite (AFG). (**d**) Excavated pit for the extraction of fluorite and barite. (**e**) Monzogranite (MG) intruding weathered granodiorite (GR).

3. Materials and Methods

Integration of field and laboratory works include field trips and a variety of analytical procedures for geochemistry and mineral chemistry, in addition to microscopic investigation. The fieldwork was performed for the collection of fresh samples on a systematic basis and field observations for lithological variation, contacts, and structural elements. For the microscopic study, representative thin- and polished sections were prepared for investigation using transmitted and reflected lights. The petrographic section pays attention to mineralogical composition, including alterations, and textures. For the whole-rock chemical analyses, the selected samples were fresh and pulverized down to less than 40 µm after crushing and coarse grinding. Analyses of major oxides and trace elements were conducted in the Geo Analytical Lab of Washington University, USA. The measurements were done by applying the Thermal Spectrometer of X-ray Fluorescence (XRF) and Agilent 7700 inductively coupled plasma mass spectrometry (ICP-MS). For accuracy and precision, the routine of duplicate samples was followed in which the XRF analytical precision is greater than 1% (2σ) for most major elements and better than 5% (2σ%) for the majority of trace elements (except Ni, Cr, Sc, V, and Cs). ICP-mass spectrometry (ICP-MS) was used to measure the concentrations of REEs in addition to Ba, Sr, Zr, Rb, Sc, Cs, Nb, Y, Hf, Ta, Pb, U, and Th. Most trace elements had detection limits that were better than 5% (2σ). This

varied for Th, U, Nb, Ta, Pb, Rb, Cs, and Sc between ±9% to ±17% (2σ). Ten polished thin sections were subjected to mineral chemistry analysis utilizing a JEOL JXA-8500F super probe housed at Washington State University. A ZAF correction program was used in order to rectify the data following the procedure recommended by [27]. Operating conditions were a 15 kV voltage acceleration, a 20 nA current beam, a focused 5-10 µm beam diameter, and on-peak counting times of 20 s. A set of natural and synthetic minerals were used as standards.

4. Petrography

The granitic rocks, including the BRC and its country rocks in the Gebel El Bakriyah area were subjected to petrographic investigation. Different rock varieties can be distinguished among the two main categories: (1) country rocks (granodiorites and monzogranite), and (2) BRC (syenogranite and alkali feldspar granites). Generally, the granodiorites are medium- to coarse-grained and show hypidiomorphic and porphyritic texture. They are essentially composed of quartz, plagioclase, microcline, and biotite with some minor zircon and allanite as accessory minerals. Plagioclase crystals are euhedral to subhedral prisms that show variable degrees of sericitization while the biotite flakes are slightly altered to chlorite with some fine apatite inclusions (Figure 3a). The monzogranite, syenogranite, and alkali feldspar granites are holocrystalline and show hypidiomorphic texture, and they are composed essentially of K-feldspar, plagioclase, quartz, biotite and hornblende while kaolinite and sericite represent secondary minerals. The percentage of mafic minerals in the three granite varieties range from 4% to 8%. They are represented by ferromagnesian minerals such as hornblende and biotite.

Accessory minerals are mostly zircon, apatite, columbite, fluorite, titanite, and Fe-Ti oxides. K-feldspars are represented by medium to coarse, subhedral to anhedral crystals that are characterized by perthite texture. Content of potash feldspars, either homogeneous or in the form of perthite intergrowth, in syenogranite and alkali feldspar granite is greater than in monzogranite. K-feldspars occur as subhedral to anhedral prisms which are represented by microcline perthite and to a lesser extent orthoclase perthite, in addition to their homogeneous counterparts. They appear turbid or cloudy at their cores where partial kaolinitic alteration can be observed. Alteration of feldspars to sericite is also seen (Figure 3b). Sericitized plagioclase and kaolinitized potash feldspars occur either as prismatic phenocrysts or as small flattened crystals with subhedral to anhedral outlines. Perthite is one of the distinctive micro-textures in the investigated syenogranite and alkali feldspar granite where three types of perthite intergrowth can be seen: namely string, vein and patchy. Some perthite crystals contain inclusions of small quartz crystals. Quartz occurs mostly in the form of subhedral phenocrysts or as medium- to coarse-sized aggregates, which fill the interstitial spaces between the feldspars. Several examples show graphic and granophyric intergrowths in quartz and potash feldspar discrete crystals (Figure 3c). Biotite is partially chloritized and occurs as dark brown flakes interstitially between quartz and feldspars. Some biotite flakes show rugged peripheries and are squeezed in between the felsic minerals. Muscovitization of biotite is common (Figure 3d). Hornblende occurs as coarse prismatic crystals that are partially altered to chlorite and encloses flakes of muscovite and perthite (Figure 3e,f). Occasionally, some simply-twinned hornblende crystals can be seen.

Metamict zoning in accessory zircon can be seen especially using high magnification. Fluorite is the most common accessory mineral, found mostly in mineral interstices occurring as subhedral to anhedral isolated crystals or in the form of veinlets. Granites in the Gebel El-Bakriyah area contain 2%–4% opaque mineral content that is represented by Fe-Ti oxides. They are homogeneous magnetite and ilmenite in which the latter shows variable degrees of martitization whereas the latter is partially replaced by secondary titanite (Figure 3g). Figure 3h shows fluorite with Nb-Ta inclusion.

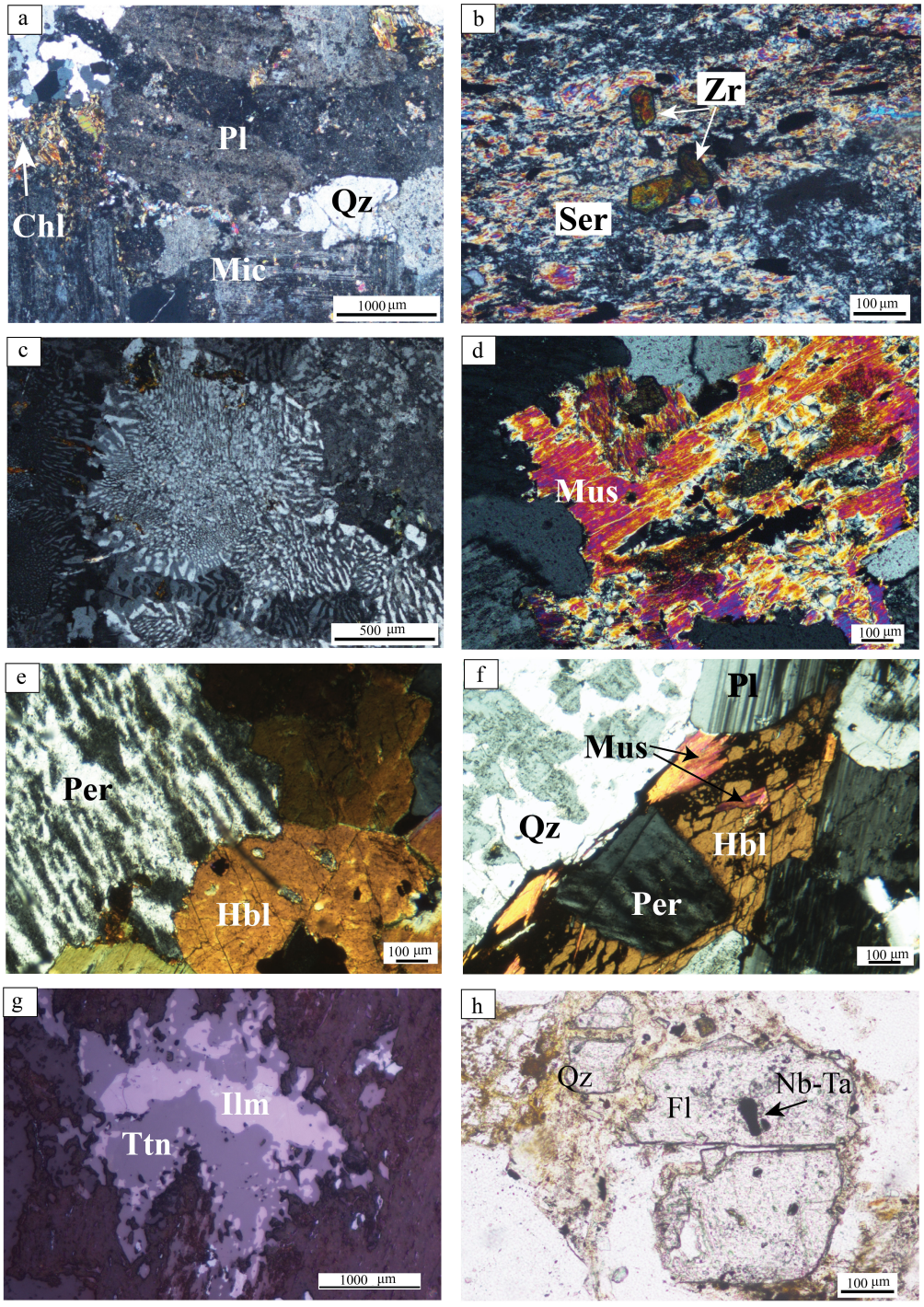

Figure 3. Photomicrographs of Gebel El Bakriyah granitic rocks. (**a**) Large plagioclase crystal (Pl), microcline (Mic), quartz (Qz), and chlorite (Chl) as primary and secondary constituents of granodiorite, Crossed-Nicols (CN). (**b**) Alteration of feldspars to sericite (Ser) and occurrence of euhedral terminated zircon in syenogranite, CN. (**c**) Intergrowths of quartz and K-feldspars to form graphic and granophyric textures in monzogranite, CN. (**d**) Muscovitization (Mus) of primary biotite in syenogranite, C.N. (**e**) Coarse hornblende (Hbl) in contact with perthite (Per) in monzogranite, CN. (**f**) Hornblende crystal (Hbl) surrounded by quartz (Qz) and plagioclase (Pl). Notice that hornblende partially encloses muscovite (Mus) and pethite (Per) in syenogranite, CN. (**g**) Homogeneous ilmenite (Ilm) extensively altered to titanite (Tnt) reaction rim in granodiorite, CN. (**h**) Fluorite (Fl) with typical cubic habit enclosing Nb-Ta minerals.

5. Whole-Rock Geochemistry

Tables 1 and 2 provide the bulk chemical composition (major, trace and REEs) of the selected samples from the country rocks and BRC. Alkali feldspar granites are characterized by SiO_2 = 69.6–72.7 wt.%), CaO (1.08–1.29 wt.%), Al_2O_3 (13.7–15.4 wt.%), TiO_2 (0.07–0.31 wt.%), and MgO (0.19–0.24 wt.%). Syenogranite has (SiO_2 = 74.3 –77.1 wt.%) with lower contents of Al_2O_3 (12.4–13.6 wt.%), CaO (0.7–1.1 wt.%), TiO_2 (0.02–0.09 wt.%), MgO (0.08–0.1 wt.%), P_2O_5 (0.01 wt.%). In the country rocks, granodiorite has a moderate SiO_2 = 63–64 wt.%) with Al_2O_3 of 15.8–16.3 wt.%, high CaO (3.56–3.58 wt.%), TiO_2 (0.63–0.69 wt.%), MgO (0.08–0.1 wt.%), and P_2O_5 (0.14–0.15 wt.%). Monzogranite distinguished by SiO_2 = 73.4–74.5 wt.%), Al_2O_3 (12.6–13.7 wt.%), CaO (0.46–0.56 wt.%), TiO_2 (0.2–0.3 wt.%), MgO (0.27–0.38 wt.%), P_2O_5 (0.04–0.07 wt.%). Also, the concentrations of trace elements in the BRC granite varieties differ from those in the country rocks. In this respect, granites of the BRC (syenogranite and alkali feldspar granite) are rich in Rb, Y, Ga, Nb, Ta, Th, and U compared to the country rocks (granodiorite and monzogranite). However, Zn and Sr are of lower amounts in syenogranite (9–27 ppm and 31–52 ppm, respectively) but high in the alkali feldspar granite (57–96 ppm and 57–70 ppm, respectively) and the country rocks (51–226 ppm and 123–272 ppm, respectively). Ba is much higher in country rocks (378–1012 ppm) compared to the BRC granites (99–326 ppm in syenogranite and 301–468 ppm in alkali feldspar granite). The total concentrations of rare-earth elements ΣREE are high in the BRC granites (ΣREEs = 180–264 in syenogranite and ΣREEs = 296–547 ppm in alkali feldspar granite) compared to those in the country rocks (ΣREEs = 103–265 ppm). To confirm the field and petrographic nomenclature of the different granitic varieties, classification of the Gebel El Bakriyah granites can be ascertained using the total alkalies vs. silica (TAS) diagram (Figure 4a) of [28]. Some of the country rocks plot in the granodiorite field while the others (monzogranite) plot in the granite field. This is supported by the use of the quartz-alkali feldspar-plagioclase (QAP) diagram proposed by [29]. According to this diagram, the country rock samples fall in the granodiorite and monzogranite fields while the BRC samples plot in the syenogranite and alkali feldspar granite fields (Figure 4b). The [30] diagram (Figure 4c) shows that all granitic samples have an alumina saturation index greater than unity indicating that they are peraluminous except granodiorite, which plots at the transition line between the metaluminous and peraluminous fields. This is evidenced by the considerable corundum content of the studied samples up to 5.92% (Supplementary File S1 (T1)). Figure 5a,b present REEs patterns (spider diagrams) normalized using the chondrite values of [31]. The REEs patterns of syenogranite and alkali feldspar granite are comparable with the country rocks in terms of much abundance in the former and magnitude of anomalies. The studied samples are characterized by LREE enrichment with nearly flat HREEs and a strongly negative Eu anomaly, particularly in the case of syenogranite and alkali feldspar granite. Figure 5c,d show spider diagrams of some trace elements normalized to values in the primitive mantle of [32]. The figure shows significant enrichment in large ion lithophile elements (LILE) as well as incompatible elements that act similarly to LILE (such as Th and U). The granites of the BRC and their country rocks are characterized by relative enrichment in Zr, Y, and Ta whereas Ti, Ni, K, and P are low. Also, granodiorite shows slight depletion in Cr.

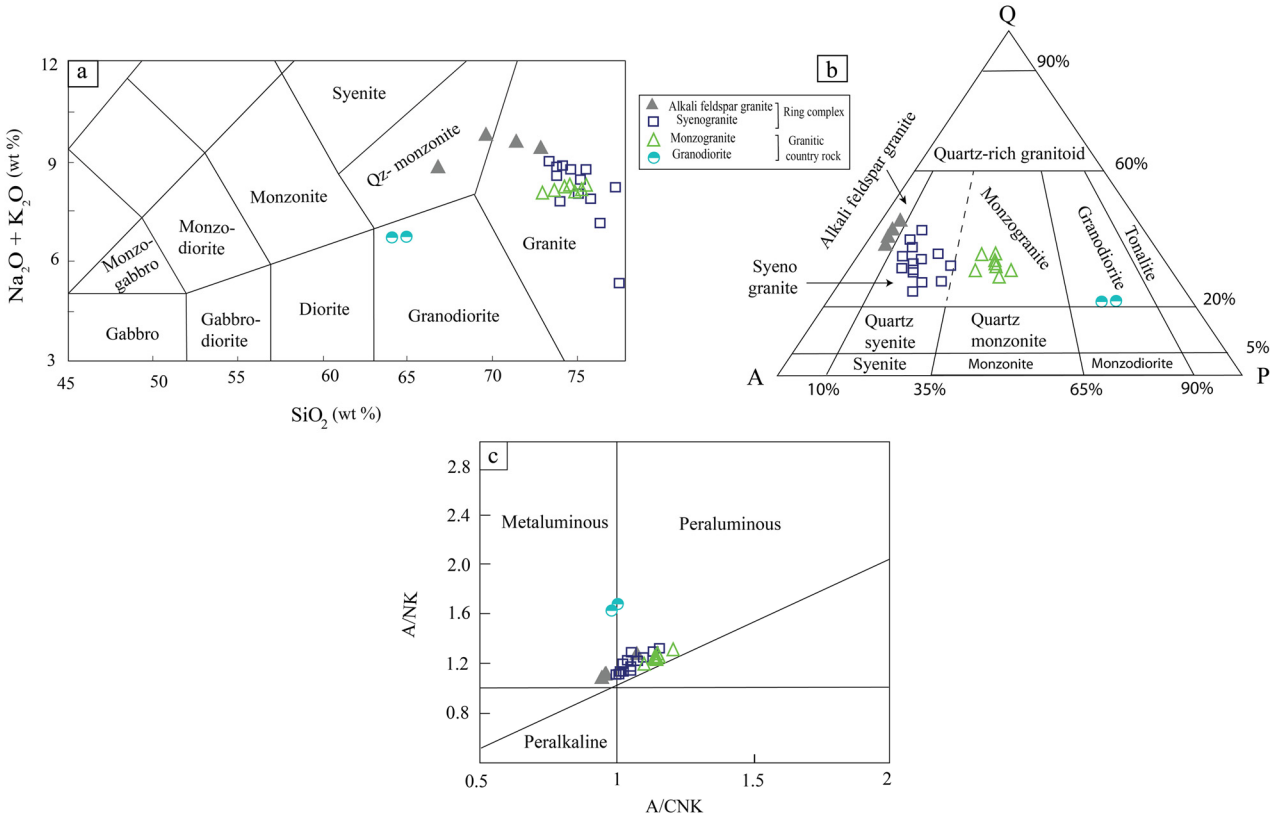

Figure 4. (**a**) Nomenclature of the granitic rocks from the Gebel El Bakriyah area using the total alkali-silica (TAS) classification diagram [28]. (**b**) Plots of the studied granitic rocks, based on their modal compositions, on the QAP diagram [29]. (**c**) Peraluminous nature of the Gebel El Bakriyah younger granites on the A/CNK vs. A/NK diagram [30].

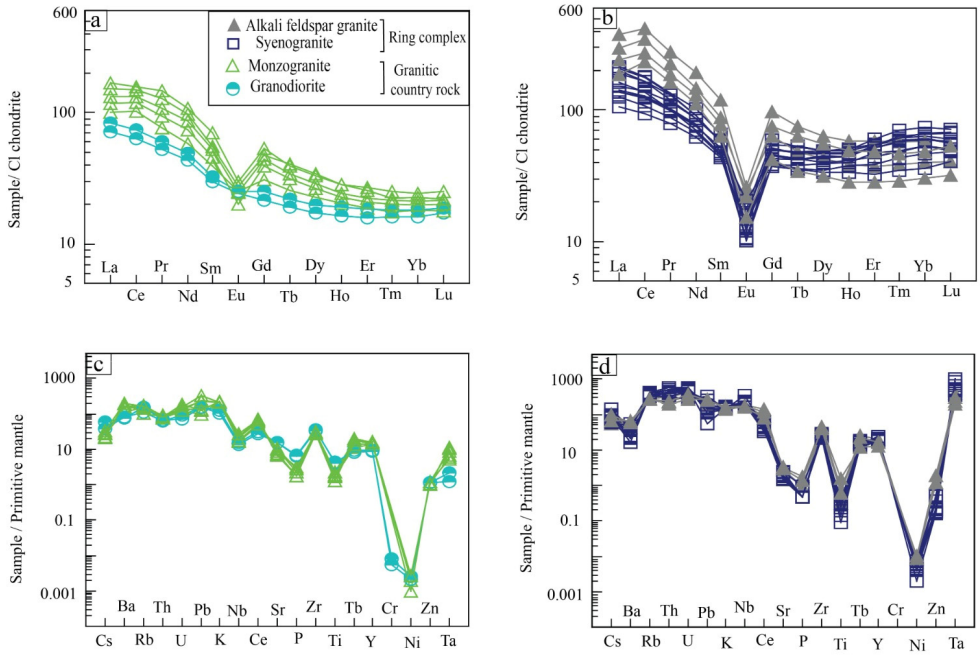

Figure 5. Spider diagrams based on trace elements and rare-earth elements (REEs). (**a**,**b**) Patterns of chondrite-normalized REEs of the Gebel El Bakriyah area [31]. (**c**,**d**) Patterns of primitive mantle-normalized multi-element variation [32].

Table 1. Whole-rock chemical composition of syenogranite of the Gebel El Bakriyah ring complex (BRC).

Sample #	FS1	FS11	FS2	FS5	FS6d	FS7	S26	S28	S29	S30	S31	S33
Major oxides (wt.%)												
SiO_2	74.33	74.74	76.32	73.91	77.88	74.84	77.18	73.56	75.65	73.41	75.28	75.08
TiO_2	0.05	0.05	0.05	0.09	0.05	0.07	0.02	0.06	0.05	0.06	0.06	0.03
Al_2O_3	13.61	13.05	12.42	13.08	12.57	13.37	12.6	13.8	12.96	13.53	13.28	12.96
Fe_2O_3	0.91	1.31	0.34	0.78	0.36	0.57	0.56	1.18	0.76	1.47	0.67	0.79
MnO	0.02	0.02	0.01	0.02	0.02	0.01	0.02	0.01	0.01	0.03	0.01	0.01
MgO	0.14	0.14	0.1	0.15	0.08	0.16	0.07	0.16	0.15	0.17	0.13	0.14
CaO	0.73	0.76	0.75	1.19	0.61	0.83	0.56	0.94	0.64	0.88	0.84	0.77
Na_2O	4.05	2.87	2.66	3.46	1.04	3.92	3.84	4.09	3.44	3.89	3.74	3.96
K_2O	4.69	5.08	4.48	4.24	4.27	4.23	4.31	4.77	4.44	4.72	4.74	4.69
P_2O_5	0.01	0.01	0.01	0.02	0.01	0.01	0.01	0.01	0.01	0.01	0.01	0.01
LOI	1.11	1.42	1.74	2.13	2.33	2.04	1.06	1.87	1.68	1.73	1.43	1.38
Total	99.65	99.45	98.88	99.07	99.22	100.05	100.23	100.45	99.79	99.9	100.19	99.82
Trace elements (ppm)												
Rb	218.94	205.71	247.81	201.62	272.77	212.06	224.59	191.59	212.44	206.48	237.84	215.57
Ba	256.83	326.31	394.28	309.47	278.8	177.01	154.51	371.04	152.34	170.52	156.51	115.23
Sr	47.61	41.79	33.59	51.97	30.75	39.74	30.92	52.09	37.8	50.73	38.58	39.96
Nb	153.67	155.18	171.82	141.83	246.72	164.96	171.76	156.52	170.69	147.39	172.34	168.27
Zr	284.54	285.62	260.56	232.17	320.55	311.42	250.38	285.32	285.19	271.93	314.08	302.31
Y	87.21	87.6	92.42	81.55	106.17	82.68	98.98	79.61	96.54	78.41	90.93	98.17
Zn	9.98	11.83	26.71	17.66	8.35	7.91	9.19	10.73	11.22	24.93	8.89	10.47
Cu	<d.l.	1.55	1.83	2.06	1.38	<d.l.	1.31	<d.l.	<d.l.	<d.l.	<d.l.	<d.l.
Ni	12.32	11.89	7.89	14.67	3.96	10.17	7.98	16.41	8.87	15.23	8.22	10.05
Co	<d.l.	<d.l.	<d.l.	<d.l.	<d.l.	<d.l.	<d.l.	<d.l.	<d.l.	<d.l.	<d.l.	<d.l.
Cr	<d.l.	<d.l.	<d.l.	<d.l.	<d.l.	<d.l.	<d.l.	<d.l.	<d.l.	<d.l.	<d.l.	<d.l.
V	16.07	14.6	12.18	15.76	9.95	12.86	10.68	15.33	13.15	16.03	13.53	12.13
Pb	12.8	11.22	9.1	22.36	7.77	10.74	9.99	17.69	3.93	18.42	13.39	10.25
Ga	40.47	35.31	43.16	33.47	44.84	35.78	40.12	31.82	40.38	34.03	39.29	37.65
Sc	<d.l.	<d.l.	<d.l.	<d.l.	<d.l.	<d.l.	<d.l.	<d.l.	<d.l.	<d.l.	<d.l.	<d.l.
Mo	1.99	1.89	2.27	1.08	4.18	1.58	2.19	1.49	3.24	1.59	1.79	1.77
Cs	0.5	0.64	0.73	0.48	1.09	0.76	0.73	0.27	0.71	0.46	0.78	0.66
Hf	7.11	7.68	9.54	9.54	11.22	9.09	8.31	6.85	7.46	9.48	7.85	11.02
Ta	17.94	18.56	26.13	14.15	42.28	20.37	33.54	17.93	21.57	19.93	20.31	19.67
Th	34.36	33.6	44.12	28.13	48.45	36.93	43.49	28.71	36.45	26.95	33.56	35.82
U	9.33	11.25	11.82	5.75	12.13	11.76	12.02	8.04	11.15	9.65	10.82	9.88
Rare-earth elements (ppm)												
La	47.42	49.33	50.94	24.93	32.51	33.56	29.69	43.86	38.88	45.19	35.73	32.74
Ce	100.95	108.81	110.64	57.33	77.4	78.11	66.13	94	84.15	100.92	85.58	75.65
Pr	12.4	12.59	12.87	7.54	9.7	9.71	8.41	10.6	9.54	11.37	10.94	9.33
Nd	42.8	42.34	47.48	29.12	35.28	36.48	31.47	38.32	32.64	40.61	40.42	35.1
Sm	8.71	8.74	10.09	6.61	7.92	7.43	6.92	8.17	7.14	9.02	8.87	7.93
Eu	0.93	0.91	1.02	0.79	1.19	0.59	0.62	1.03	0.74	0.7	0.78	0.61
Gd	11.15	10.61	12.24	7.67	8.81	7.96	7.95	9.48	9.44	10.31	10.22	9.21
Tb	1.99	1.75	1.95	1.32	1.56	1.42	1.35	1.62	1.59	1.78	1.8	1.56
Dy	12.35	11.9	12.45	8.57	11.35	10.05	8.78	10.95	10.21	12.07	12.53	11.01
Ho	2.76	2.62	2.86	1.91	2.49	2.27	2.16	2.37	2.33	2.66	2.83	2.52
Er	8.94	8.54	9.17	5.36	8.91	7.79	6.43	7.57	7.27	8.59	9.91	9.02
Tm	1.52	1.46	1.55	0.89	1.61	1.25	1.11	1.25	1.22	1.48	1.78	1.55
Yb	10.31	10.4	10.78	6.08	11.16	9.01	7.96	8.81	9.01	10.12	12.52	11.38
Lu	1.42	1.43	1.53	1.04	1.71	1.25	1.23	1.26	1.29	1.47	1.83	1.72
Eu*	10.39	10.49	11.4	7.06	8.76	8.49	7.63	9.31	8.25	10.13	9.85	8.6
Eu/Eu*	4.12	4.04	4.17	4.12	4.03	4.29	4.13	4.12	3.95	4.01	4.1	4.08
$(La/Yb)_n$	3.84	3.93	4.81	5.25	5.44	4.74	6.76	3.79	5.01	3.14	3.39	3.97
$((La/Sm)_n$	2.77	2.67	3.43	3.73	4.99	3.8	5.17	2.71	3.82	2.37	3.07	3.84
$(Gd/Lu)_n$	5.73	5.99	6.51	7.43	4.92	5.94	6.23	6.54	5.85	6.09	4.98	5.12
$(La/Lu)_n$	22.61	23.01	28.46	31.61	30.09	29.54	39.18	22.97	29.88	18.21	18.85	23.11
T1.3	1.04	1.04	0.99	1.02	1.06	1.04	0.99	1.02	1.02	1.04	1.04	1.02
ΣREEs	263.65	271.43	285.57	159.16	211.6	206.88	180.21	239.29	215.45	256.29	235.74	209.33
Y/Ho	31.6	33.44	32.31	42.7	42.64	36.42	45.82	33.59	41.43	29.48	32.13	38.96
T (°C) Zr	842	852	850	824	905	854	834	837	852	835	851	843

Table 2. Whole-rock chemical composition of the other granites forming the Gebel El Bakriyah ring complex (BRC).

	Alkali Feldspar Granite		Monzogranite										Granodiorite	
Sample #	**FS13**	**FS13A**	**S7b**	**S35A**	**S8**	**S13**	**S18**	**S20**	**FS23**	**S39**	**FS12**	**FS15**	**S35b**	**S1**
Major oxides (wt.%)														
SiO_2	72.78	69.66	66.64	71.19	73.68	74.37	74.48	74.12	74.53	75.42	74.37	75.52	64.9	63.92
TiO_2	0.07	0.18	0.33	0.13	0.31	0.29	0.36	0.31	0.26	0.21	0.29	0.29	0.66	0.69
Al_2O_3	13.78	14.12	15.48	14.34	13.45	13.09	13.77	12.76	13.17	12.87	13.09	12.61	16.31	15.86
Fe_2O_3	1.82	2.93	3.21	2.28	1.79	1.45	1.28	1.56	1.58	1.3	1.45	1.21	4.72	4.81
MnO	0.03	0.06	0.09	0.03	0.03	0.01	0.02	0.04	0.05	0.03	0.01	0.04	0.08	0.07
MgO	0.19	0.21	0.24	0.2	0.33	0.32	0.38	0.35	0.3	0.27	0.32	0.31	1.72	1.69
CaO	1.02	1.11	1.29	1.08	0.56	0.54	0.55	0.56	0.52	0.46	0.54	0.49	3.56	3.58
Na_2O	4.56	4.64	4.48	4.59	3.49	3.44	3.37	3.43	3.53	3.45	3.44	3.28	4.16	4.41
K_2O	4.88	5.04	4.37	5.01	4.58	4.78	4.54	4.44	4.64	4.75	4.78	4.67	2.74	2.28
P_2O_5	0.02	0.04	0.12	0.03	0.06	0.05	0.07	0.04	0.04	0.04	0.05	0.04	0.15	0.14
LOI	1.22	1.36	2.91	1.23	1.25	1.52	1.12	0.92	0.83	1.02	1.52	1.33	1.14	1.95
Total	100.37	99.35	99.16	100.1	99.53	99.86	99.94	98.53	99.45	99.82	99.86	99.79	100.1	99.4
Trace elements (ppm)														
Rb	179.66	170.87	167.2	172.4	56.26	79.86	96.66	84.48	81.84	90.86	60.48	122.49	80.77	60.48
Ba	300.73	409.67	468.4	402.5	1012.6	765.5	812.5	768.0	551.9	977.3	404.1	741.54	378.2	404.1
Sr	57.14	66.7	69.84	61.42	189.64	175.8	153.1	139.7	126.3	123.5	272.6	133.71	267.9	272.6
Nb	132.41	124.59	112.6	119.6	9.89	9.05	11.71	11.53	13.03	15.21	7.65	19.27	8.38	7.65
Zr	372.31	512.18	507.4	439.5	257.33	256.4	243.6	240.3	236.9	224.8	282.6	217.75	290.2	282.6
Y	88.55	75.33	56.89	76.89	47.68	46.79	48.82	46.28	51.51	54.58	29.97	57.69	30.78	29.97
Zn	57.24	96.41	60.88	92.11	52.79	59.03	203.9	226.3	60.04	51.28	56.46	75.51	57.78	56.46
Cu	<d.l.	<d.l.	<d.l.	<d.l.	5.97	4.79	4.43	3.76	3.68	2.71	10.76	2.33	11.71	10.76
Ni	16.42	18.17	21.05	17.22	5.49	3.91	2.04	<d.l.	<d.l.	<d.l.	5.03	<d.l.	4.15	5.03
Co	<d.l.	2.24	3.1	<d.l.	4.46	3.07	<d.l.	2.14	2.72	1.5	9.52	2.42	10.28	9.52
Cr	<d.l.	<d.l.	<d.l.	<d.l.	<d.l.	<d.l.	<d.l.	<d.l.	<d.l.	<d.l.	24.33	<d.l.	16.47	24.33
V	17.03	18.37	19.62	16.98	34.97	28.74	29.26	21.61	22.3	12.14	47.76	9.18	45.54	47.76
Pb	12.79	16.37	18.66	17.61	27.9	11.66	27.01	37.93	16.03	14.66	18.56	15.02	17.66	18.56
Ga	36.11	31.05	27.29	35.77	20.04	19.23	20.59	21.93	24.04	22.23	21.36	25.13	21.59	21.36
Sc	<d.l.	<d.l.	<d.l.	<d.l.	0.57	0.53	0.46	0.48	0.31	0.24	7.01	0.19	6.86	7.01
Mo	5.05	5.12	4.75	4.03	0.94	1.44	1.88	2.32	2.38	2.04	2.25	3.37	1.57	2.25
Cs	0.83	0.43	0.51	0.79	0.38	0.48	0.41	0.52	0.48	0.59	0.69	0.65	1.05	0.69
Hf	12.68	13.18	12.96	10.53	6.67	6.27	7.09	6.76	6.66	7.11	4.72	7.37	5.57	4.72
Ta	16.55	9.74	8.05	12.23	0.25	0.22	0.28	0.44	0.35	0.47	0.05	0.59	0.09	0.05
Th	26.25	18.71	16.44	20.44	5.27	4.83	5.35	4.74	5.73	5.24	3.96	6.34	4.12	3.96
U	8.75	7.21	5.61	7.66	2.22	2.16	2.48	2.76	2.42	3.21	1.6	3.78	1.25	1.6
Rare-earth elements (ppm)														
La	88.63	57.59	44.24	69.85	27.84	24.03	36.13	31.34	43.27	39.91	16.88	41.65	19.68	16.88
Ce	257.77	166.45	142.7	212.9	73.07	63.12	91.23	81.61	101.8	96.42	38.66	101.95	45.21	38.66
Pr	26.29	17.63	15.35	21.45	8.98	7.27	12.24	10.21	11.6	13.84	4.97	13.99	5.7	4.97
Nd	90.14	60.51	52.3	68.63	34.48	27.01	45.41	40.3	41.86	50.34	20.28	52.59	22.97	20.28
Sm	18.25	12.02	9.66	13.49	7.03	5.99	8.44	7.98	9.51	10.8	4.59	11.02	4.95	4.59
Eu	1.52	1.42	0.88	1.28	1.16	1.47	1.58	1.44	1.82	1.74	1.41	1.91	1.45	1.41
Gd	19.9	13.06	8.64	15.46	8.04	6.36	9.78	9.12	11.17	10.94	4.39	13.81	5.17	4.39
Tb	2.81	1.81	1.29	2.37	1.17	0.95	1.53	1.29	1.72	1.48	0.71	2.04	0.82	0.71
Dy	16.16	10.88	7.97	14.01	6.73	5.79	8.72	7.37	9.56	8.46	4.41	11.59	5.04	4.41
Ho	3.31	2.18	1.61	2.77	1.28	1.15	1.6	1.38	1.79	1.6	0.93	2.2	1.08	0.93
Er	9.66	6.16	4.69	7.95	3.42	3.12	4.44	3.67	4.79	4.26	2.63	5.53	3.05	2.63
Tm	1.46	0.99	0.74	1.18	0.51	0.45	0.64	0.55	0.69	0.57	0.41	0.79	0.46	0.41
Yb	9.82	6.76	5.17	8.22	3.38	3.06	4.13	3.59	4.63	3.86	2.74	5.34	3.07	2.74
Lu	1.6	1.03	0.81	1.35	0.51	0.45	0.64	0.55	0.68	0.56	0.44	0.8	0.48	0.44
Eu*	21.9	14.56	12.18	17.01	7.95	6.6	10.16	9.03	10.5	12.23	4.78	12.42	28.54	81.48
Eu/Eu*	4.12	4.16	4.29	4.03	4.34	4.09	4.47	4.46	3.99	4.12	4.25	4.24	0.88	0.27
$(La/Yb)_n$	2.72	3.04	3.51	2.57	1.54	1.55	1.2	1.29	1.2	1.23	1.51	1.15	4.33	5.75
$((La/Sm)_n$	1	1.06	1.07	0.95	0.59	0.66	0.44	0.46	0.49	0.38	0.8	0.45	2.51	3.27
$(Gd/Lu)_n$	12.5	12.14	13.05	11.43	13.78	13.31	13.19	14.51	13.78	18.95	11.2	13.95	1.32	1.4
$(La/Lu)_n$	17.98	18.9	22.22	17.32	10.33	10.73	8.36	8.62	8.3	9.19	9.66	8.03	4.2	5.3
T1.3	1.08	1.08	1.13	1.15	1.05	1.06	1.08	1.04	1.06	1.03	1	1.04	1	1.15
ΣREEs	547.32	358.49	296.0	441	177.6	150.2	226.5	200.4	244.9	244.7	103.4	265.21	119.1	103.4
Y/Ho	26.75	34.56	35.34	27.76	37.25	40.69	30.51	33.54	28.78	34.11	32.23	26.22	28.5	32.23
T (°C) Zr	851	878	892	858	842	839	842	833	832	827	848	825	821	815

6. Mineral Chemistry

For a better understanding of the mineral composition of the younger granites and its use to deduce some petrogenetic parameters, we analyzed the major silicate minerals and some non-silicates in the four granitic varieties using the electron microprobe. They include feldspars (plagioclase and K-feldspars), biotite, chlorite, amphibole, apatite, zircon, Nb-Ta oxides, and Fe-Ti oxides. Structural formulae were calculated using the Minpet software [33] together with some Excel spreadsheets.

6.1. Feldspars

Electron microprobe analyses (EMPA) of the feldspar-group minerals, their structural formulae, and end-members (mole%) are given in Supplementary File S1 (T2). The analyzed feldspars in the Gabal El Bakriyah younger granites are distinguished into K-feldspars (homogeneous orthoclase/microcline and perthite), in addition to sodic plagioclase. In the monzogranite, homogeneous K-feldspars have a high and narrow K_2O range (15.29–16.22 wt%), and therefore orthoclase component is remarkably high (89–97 mole%) while its albite component never exceeds 8 moles%. On the other hand, the range of K_2O in perthite is lower and wide (3.59–12.36 wt%), which results in a wide range of orthoclase components (20–67 mole%) and high albite components up to 76 moles%. In the syenogranite, its homogeneous K-feldspars have the highest orthoclase (95–98 mole) and lowest albite (up to 5 moles%) owing to a high and narrow K_2O range (15.57–16.32 wt%). The alkali feldspar granites have homogeneous K-feldspars (14.97–16.22 wt% K_2O, 82–97 mole% orthoclase, and up to 17% mole% albite) and few perthites (12.46–12.53 wt% K_2O, 74–75 mole% orthoclase, and up to 25 moles% albite).

The analyzed plagioclase in monzogranite is mainly sodic (9.2–10.3 wt% Na_2O), which is equivalent to 82–88 mole% albite, while anorthite in solid solution is much lower (up to 12.6 mole%) due to the low CaO content (2.2–3.2 wt%). EMPA of homogeneous plagioclase in the three granite varieties shows similarities. In the monzogranite, plagioclase contains 10.13–12.14 wt% Na_2O equivalent to high albite solid solution component amounting to 89–99 mole%. Similarly, the syenogranite (10.39–11.56 wt% Na_2O and 99 moles% albite) and the alkali feldspar granite (10.89–11.65 wt% Na_2O and 96–99 mole % albite). A second generation of homogeneous plagioclase is slightly calcic and has 9.27–10.39 wt% Na_2O and accordingly, the lowest albite component (84–89 mole%), which is typical of an oligoclase composition. On the ternary phase diagram for the classification of feldspars based on their chemistry [34], the analyzed feldspars from BRC granites plot in the orthoclase/microcline and albite field. On the other hand, feldspars from country rock lie in orthoclase/microcline, oligoclase, and anorthoclase fields (Figure 6a).

6.2. Biotite

The major primary ferromagnesian mineral in the investigated granites is biotite. Its EMPA and structural formula are presented in the Supplementary File (T3). Analyses of biotite indicate 9.5–12.8 wt% Al_2O_3, 2.4–3.9 wt% TiO_2, and 0.08–0.5 wt% MnO. Biotite in the alkali feldspar granite has a higher content of FeO^t (30.6–33.7 wt%) compared to the monzogranite (19.5–23.6 wt%) and syenogranite (~20–24.1 wt%). On the other hand, biotite from the alkali feldspar granite and monzogranite has a higher MgO content (8.6–11.9 wt%) than in the alkali feldspar granite (2.9–4.4 wt%). The FeO^t/MgO ratio ranges from 8 to 11 in the alkali-feldspar granite, which is noticeably higher than those in the syenogranite and monzogranite (0.94 to 2). On the TiO_2–FeO^t–MgO ternary diagram of [35], all analyses pertain to primary/magmatic biotite (Figure 6b). According to the classification of [36], biotite from BRC granites plot in Mg and Fe biotite whereas biotite from the country rock granites lie in the Mg-biotite field (Figure 6c).

6.3. Amphibole

For the amphibole EMPA (Supplementary File S1 (T4)), the structural formula is calculated on an anhydrous basis assuming 23 oxygen atoms per half-unit cell. Data in this file indicates that the content of FeO^t (30.41–35.35 wt%) in the monzogranite country rock is much higher than in the syenogranite or the core of the BRC (17.82–17.97 wt%). Similarly, MgO is much higher in the monzogranite (11.56–11.97 wt%) than in the syenogranite (0.44–2.53 wt%). On the classification diagram of [37] (Figure 6d), the analyzed amphibole in BRC granites is Ca-Na amphibole whereas it is Na to Na-Ca amphibole in the granites from the country rocks, i.e., it is an alkali amphibole with some Ca in the double-chain structure, specifically in the Y-sites where divalent cations are allocated. Careful application of some Excel spreadsheets enables the exact nomenclature of amphibole. As

given at the Supplementary File S1 (T4), the analyzed amphiboles comprise ferro-richterite, katophorite, ferobarrroisite, and arfvedsonite in the syenogranite. In monzogranite, it has the composition of normal arfvedsonite and Mg-arfvedsonite only.

6.4. Nb-Ta Oxides

It was possible to record and analyze Nb-Ta oxides as primary magmatic phases in the syenogranite variety only (Supplementary File S1 (T5)). These oxides are either columbite or tantalite as end-members of a solid solution series common in rare-metal granites. The analyzed columbite has high Nb_2O_5 content (42.58–69.56 wt%) than those in tantalite (21.35–24.89 wt%). Oppositely, Ta_2O_5 content in tantalite (55.38–59.71 wt%) is much higher than in columbite (8.27–38.96 wt%). MnO content in the columbite is higher than in the tantalite (up to 13.96 wt% and up to 9.77 wt%, respectively). Contents of Si, Al, and Ca oxides in the columbite-tantalite are negligible. The Ta/(Nb + Ta) ratio in tantalite is doubled compared to columbite (0.57–0.63 and up to 0.27, respectively). According to the binary classification diagram of Nb-Ta oxides based on the Mn/(Mn + Fe) vs. Ta/(Ta + Nb) ratios, the analyzed columbite is manganoan (i.e., Mn-columbite) and so is tantalite (Mn-tantalite) as shown in Figure 6e.

6.5. Zircon and Apatite

Zircon is a common accessory mineral in the investigated three granite varieties (Supplementary File S1 (T6)). The analyses show limited variations in the chemical composition in which ZrO_2 content in the BRC granites and its country rocks ranges from about 60.9 to 64.4 wt%. The range of SiO_2 content is also narrow (31 to 32 wt%). This zircon is poor in Al_2O_3 and FeO^t. In general, oxide impurities in the analyzed zircon are negligible and amount < 0.5 wt%. Because Hf_2O_3 was not among the protocol of the electron microprobe session for zircon, the sum of oxides is somehow low (95.62–98 wt %).

Apatite in the monzogranite and alkali feldspar granite varieties was analyzed (Supplementary File S1 (T6)). Apatite in the alkali feldspar granite has lower contents of CaO (44–48 wt%) and P_2O_5 (34–36 wt%) than in the monzogranite (51–56 wt% and 38–41 wt%, respectively). The analyses do not show any significant chemical variations. For example, Mn^{2+} in the apatite structure reaches up to 0.3 atoms per formula unite (apfu) in the apatite from alkali feldspar granite, which is almost the same in the apatite from monzogranite (3.2 pfu). Similarly, apatite in the two granite varieties has almost constant Ca^{2+} (10.7–11.7 apfu). The remaining oxides are present as impurities in trace levels, which do not exceed 0.5 wt%.

6.6. Fe-Ti Oxide

The chemical analyses and structural formulae of the different Fe-Ti oxides are given in the Supplementary File S1 (T7). They include magnetite, ilmenite and goethite. The abundance of magnetite is limited in the monzogranite as well as in the alkali feldspar granite, while ilmenite and goethite are restricted to monzogranite. Magnetite in the BRC granites has FeO^t in the range from 8 wt% to 92.2 wt% whereas the same range in the country rock is 86.5–92.1 wt%.

Negligible amounts of other oxide impurities (<0.5 wt%) are also noticed. In the ilmenite crystals, TiO_2 content is very narrow and ranges from 49 wt% to 50 wt% and has the expected FeO^t content in ilmenite that is noticeably wide in range (29 to 43 wt%). In some instances, the FeO^t content abruptly increases to the amount from 87 to 91 wt% in crystals with minute hematite exsolution (hematite-ilmenite exsolution or primary texture). Appreciable amounts of Mn cations are encountered in the ilmenite structure (3–8.5 wt% MnO) that is a function of a significant amount of manganese in solid solution with end-members (Mn- and Mg-ilmenite); namely geikielite ($MgTiO_3$) or pyrophanite ($MnTiO_3$). The analyzed goethite from the monzogranite shows extremely limited variations in the chemical compositions, in which FeO^t ranges from 59 to 73 wt% and the much lesser SiO_2

content is appreciable (3.8 to 5.5 wt%) and connected to increased silica activity during oxidation of magnetite.

6.7. Chlorite

As a hydrous phyllosilicate mineral, which is a secondary phase replacing biotite, its structural formula is calculated from the EMPA based on 11 oxygen atoms (Supplementary File S1 (T8)). Analysis of chlorite from the monzogranite shows high SiO_2 (27–32 wt%), Al_2O_3 (11–13wt%), FeO^t (24–29 wt%) and MgO (8.8–12.1 wt%). The contents of K_2O (up to 4.3 wt%) are moderate whereas the chlorite is poor in CaO, NaO, TiO_2, and MnO oxides. The ratio of Fe/Fe + Mg in the analyzed chlorite is a bit wide (0.5–0.9 wt%). Fe^{2+} (up to 5.4 apfu) is appreciable and greatly exceeds Fe^{3+} (0.2 apfu). According to the classification by [38], the analyzed chlorite plots in the diabantite field except for a few pycnochlorite compositions (Figure 6f).

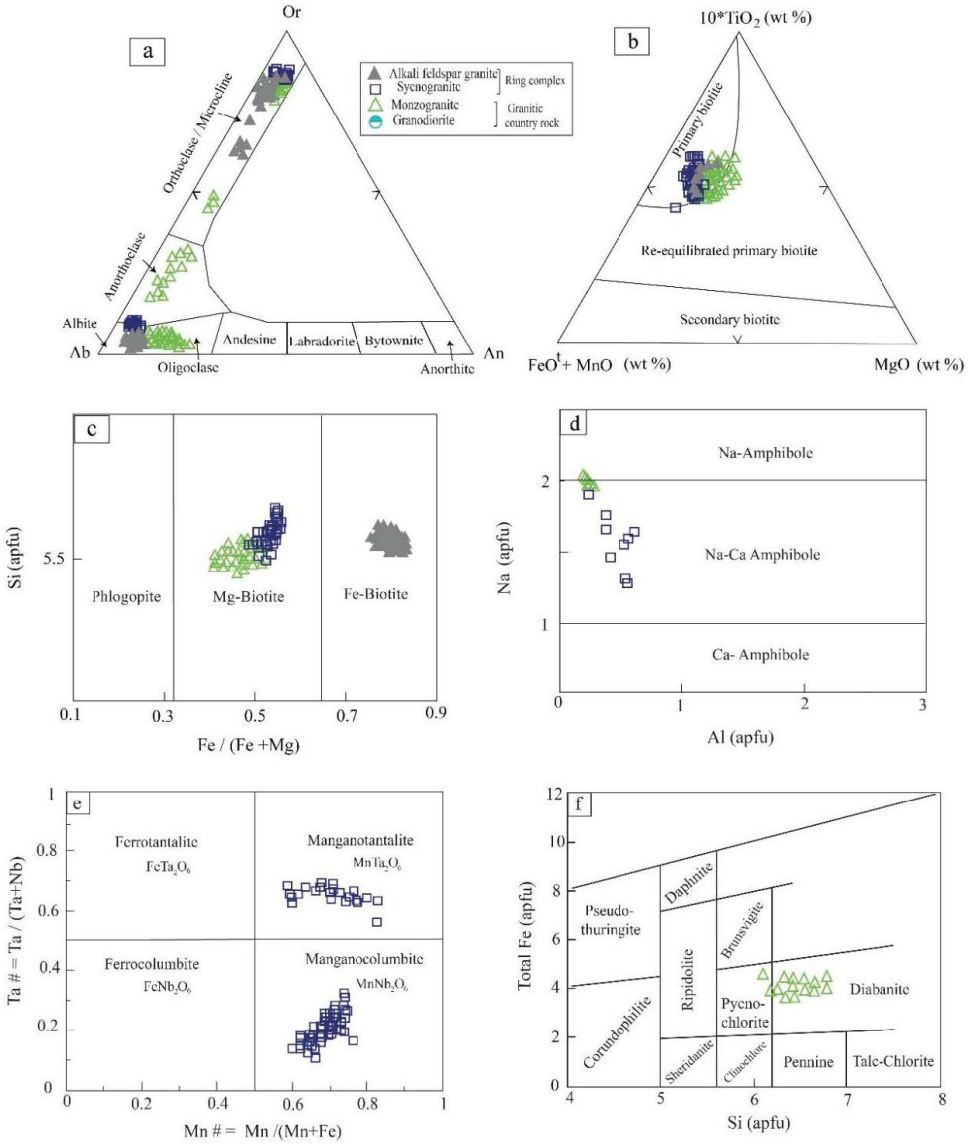

Figure 6. (**a**) Composition of the feldspars in Gebel El Bakriyah granitic rocks using the Ab-Or-An ternary diagram of [34]. (**b**) The primary origin of biotite is based on the (FeO^t + MnO)–10*TiO_2–MgO discrimination diagram of [35]. (**c**) Nomenclature of biotite (Fe- and Mg-bearing) using the classification of [36]. (**d**) Na-Ca amphibole plots after [37]. (**e**) Mn-rich end-members of the Nb-Ta oxides. (**f**) Chlorite composition in the Gebel El Bakriyah granitic rocks [38].

7. Discussion

7.1. Conditions of Magmatic Crystallization

The mineral assemblages and the physico-chemical properties of the magma are closely related during the crystallization process [39]. Temperature (T), pressure (P), and oxygen fugacity (f_{O_2}) all have a significant impact on the mineral compositions and crystallization histories of magmatic systems. Zircon exhibits variable behavior in felsic rocks and is frequently concentrated in residual silicate melts until zircon saturation occurs [40]. For the felsic magmas, [40] used the relationship between the solubility of zircon and crystallization temperature with major element composition in the melt to determine their temperature. According to the calibration of [40], the assessed Zr saturation temperature for the studied granitic rocks from the BRC ranges from 824 to 905 °C while the temperature of the country rocks is between 815–848 °C.

Based on the norm calculations given in the Supplementary File S1 (T1), an Ab-Or-Qz ternary diagram (Figure 7a) was constructed, which shows that the studied granites evolved in extremely low H_2O vapor pressures where the samples plot near the lowest point of the diagram between 2–6 kbar. The analyzed biotites in the country rock and the BRC granites have low TiO_2, which indicate low-pressure condition of the granite emplacement for all varieties [41]. This gives evidence that the condition of crystallization for the BRC occurred at a shallow depth condition in the crust.

According to [42], oxygen fugacity (f_{O_2}), is an important factor controlling magmatic activity that may be used to determine the redox conditions of melts during petrogenesis. Since magnetite frequently becomes Ti-free during slow cooling and ilmenite generally through one or more oxidation processes, it is difficult to determine the initial oxygen fugacity of the the primary magma [43]. However, amphibole chemistry can be used as a petrogenetic indicator for oxygen fugacity (f_{O_2}). The chemistry of amphiboles in the Gebel El-Bakriyah syenogranite (the core of the BRC) indicates a low f_{O_2} (Figure 7b) that refer to a reducing condition upon magmatic crystallization until the minor metasomatic changes at the late stage, more likely deuteric alterations. Evolution of A-type granite includes fractionation of felsic melts in low f_{O_2} condition [44]. This is supported by low Mg# (0 to 0.04) ratio and low TiO_2 along with high Al_2O_3 content in biotite.

7.2. Magma Type and Tectonic Setting

It is possible to deduce the magma type of the studied granites using either composition of these rocks, i.e., the whole-rock analysis, or with the aid of some rock-forming minerals (e.g., micas) as petrogenetic indicators. The chemical compositions of biotite and saturation index of alumina (Figure 7c) indicated that the investigated country rocks represented by monzogranite have calc alkaline character while the BRC granites have an alkaline nature. Alumina saturation index indicates the peraluminous nature for most of the studied granites, which is confirmed by high normative corundum up to 5% (Figure 4c and Supplementary File S1 (T1). Some geochemical characteristics such as high contents of Nb, Ta, Y, Zr, Th, considerable Ga/Al ratio and remarkable depletion in MgO, CaO, and P_2O_5 categorize most of the younger granites in the Gebel El-Bakriyah area as A-type granites [10]. Alkali feldspar granite and syenogranite have a ferroan nature representing the alkaline A-type character of the BRC while monzogranite and granodiorite have a magnesian nature (Figure 7d). Some geochemical parameters can be used to examine the Gebel El Bakriyah granitic rocks to determine the tectonic setting for their origins. Based on the whole-rock geochemistry, the Gebel El Bakriyah granites cover the range from volcanic-arc for the granodiorite samples followed by a transitional phase as shown by the monzogranite samples to post-collision (within-plate) granites for the BRC according to the tectonic discrimination diagrams of [45] (Figure 7e).

Generally, the peraluminous granites, which is the case of the El Bakriyah area are often produced as a result of collisional (country rocks) and/or post-collisional (BRC) conditions [46]. However, the A-type rocks of the Gebel El-Bakriyah granites have general geochemical characteristics of calc-alkaline (country rocks) to alkaline (BRC) magma

evolved in a collisional to post-collisional stage. This is evidenced by a high content of SiO_2, notable depletion in CaO, MgO, and Sr with a high concentration of alkalis content, and considerable enrichment in Nb, Zr, Y, Hf, Th, in addition to REEs patterns with distinct negative Eu anomalies [10,45,47].

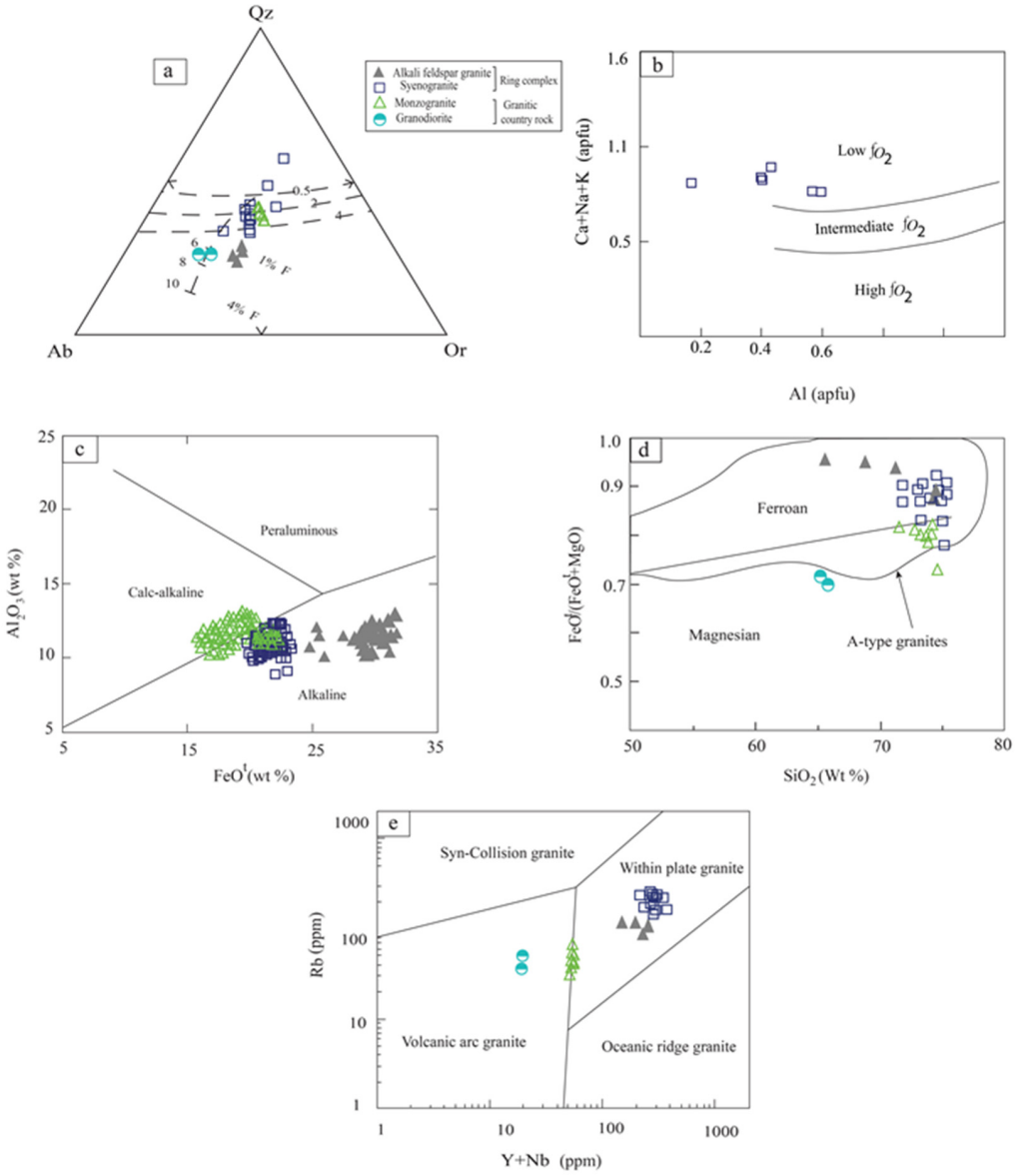

Figure 7. (**a**) The Ab–Or–Qz normative diagram of the studied granitic rocks [48] (over a pressure range from 0.5 kbar to 10 kbar of water-saturated melt) [49]. (**b**) Plots of amphibole composition indicating crystallization in low oxygen fugacity (low f_{O2}) magmatic condition [50]. (**c**) Calc-alkaline and alkaline magma composition for the different granite varieties using the contents of FeO^t and Al_2O_3 in biotite [51]. (**d**) Plots of SiO_2 vs. (FeO^t/(FeO^t + MgO) for the Gebel El Bakriyah younger granites show a ferroan nature that confines the A-type granite field [52]. (**e**) Rb vs. Y + Nb tectonic discrimination diagram for the Gebel El Bakriyah granites [45].

7.3. Magma Source and Magmatic vs. Metasomtic Process

The granitic rocks of the Eastern Desert of Egypt show a wide variation in major and trace element concentrations, which strongly suggests that a set of processes and sources were involved in their generation and emplacement [53]. Generally, three major magmatic rock units are present in the Gebel El Bakriyah area including an arc rock association represented by the older granitoids, which are intruded by the fresh post-collisional asso-

ciations of younger gabbros and the younger granites. The latter are distinguished into (1) monzogranite country rock (side by side with granodiorite of the older granitoids), and (2) syenogranite and alkali feldspar granites forming the BRC.

There are four hypotheses for the petrogenesis of A-type granites as follows: (1) fractional crystallization of lower crustal minerals after partial melting (King 2010 [54]), (2) Mantle-derived mafic magma fractional crystallization [55], (3) lower crustal constituents contaminate mafic mantle-derived melt [47], and (4) melting from the lower crust mixed with some mantle-derived materials [54].

Peraluminous granites can form as a result of fractional crystallization or partial melting of intermediate and mafic rocks or metasedimentary rocks with low total alkali and high Al concentrations, as well as magma mixing and crustal contamination [56,57]. The depletion of Ti, Ba, P, and Eu in the investigated samples of both country rocks and BRC (Figure 5) may support the fractionation of plagioclase and K-feldspar in addition to fractional crystallization of ilmenite and apatite. There is an extensive crystal fractionation in the BRC compared to country rocks, which is evidenced by the enrichment in Rb, Nb, Ta, Zr, Hf, Th, and U in the BRC.

The REEs patterns of the BRC granites show significant degrees of REEs fractionation, with a considerable enrichment in light elements (LREEs) to heavy elements (HREEs) (Figure 5), in addition to a remarkably higher some of the rare-earth elements (∑REEs) compared to the country rock granites. Zircon is spatially associated with thorite, fluorite, and columbite, indicating that these minerals are all formed from a fluid-rich, highly fractionated magma [58]. The Fractional crystallization process in the country rocks and BRC is supported by the plots of the samples on the Th/Nb vs. Zr and Ta vs. Nb diagrams (Figure 8a,b). Normally, the Zr/Hf and Nb/Ta ratios are relatively unchanged in regular magmatic processes, but they significantly change during severe magmatic fractionation when magmatic melt interacted with fluids in particular (e.g., [59]). The BRC granites exhibit a wide range of Nb/Ta ratios (6.11–13.6 and Zr/Hf ratios (16.1–26.7), which indicate fractionation and interaction between fluids and the magmatic melt. The presence of fluorite as a major interstitial accessory mineral in the investigated granites suggests that the magma was F-rich, especially during the late stage of fractional crystallization imposing an impact on the physicochemical characteristics of the felsic magma. Fluorite reduces the solubility of water in magma, as well as its viscosity, and decreases the crystallization temperature in the magma reservoir e.g., [60]. Also, the presence of rare metals, e.g., Nb and Ta, are as used as markers for extensive crystal fractionation in the melt [61]. However, the studied samples exhibit a variable increasing trend of La/Sm and La/Yb ratios versus La abundance (Figure 8c) suggesting that partial melting might have an impact on the evolution of the BRC and its country rocks in the Gebel El Bakriyah area, which is also consistent with the peraluminous nature of the investigated rocks. The role of the fractional crystallization and partial melting in the formation of the country rocks and BRC is supported by the diagram of Ni vs. Rb (Figure 8d). Finally, it can be concluded that fractional crystallization is the most acceptable process for the generation of the Gebel El Bakriyah alkaline rocks. Regardless the limited influence, the role of partial melting cannot be totally discarded, which needs more detailed isotopic evidence in the future hopefully.

The magmatic origin of the studied granitic rocks from El Bakriyah area appears to be mixing of clay-poor, plagioclase-rich, and clay-rich, plagioclase-poor along with amphibolite-rich sources (Figure 9a; [62]), which indicates that the magma originated from a mixture of metasedimentary and igneous sources, including metagraywacke and pelite for the BRC, and slightly mafic-derived melts for the country rocks (Figure 9b). We used some of our mineral chemistry data, particularly those of amphibole and biotite to confirm the source of melt that produced the Gebel El Bakriyah A-type granites. Figure 9c,d suggest post-collisional magma that formed the alkali feldspar granite, and the syenogranite was derived from a crustal source while the monzogranite of the country rocks was derived from crust-mantle mixed source.

Here, we report evidence for a few metasomatic features in the investigated El-Bakriyah granites. They include some hydrothermal alterations by late-stage fluids. In some instances, and based on the petrographic study, graphic texture (Figure 3d) represents the intergrowth of quartz and alkali feldspar formed by a possible metasomatic replacement. Nevertheless, the formation of graphic texture by exclusive eutectic crystallization in proper magmatic conditions cannot be excluded [63]. Isovalence elements have the same radius and charges (CHARC) such as Y/Ho ratios, which are stable in ortho-magmatic melt except might practice metasomatic changes. The Isovalence Y/Ho ratio amounting to 28.1 is very characteristic of chondrites that show a CHARC behavior [32]. The Y/Ho ratio in the BRC granites is higher (average-36.5), which is a non-CHARC character. The non-CHARC character of the investigated El-Bakriyah granites is likely attributed to some metasomatism, which is accepted for highly fractionated magmas exhibiting enrichment of H_2O, Li, F, B, and Cl, which implies a non-CHARC character [64]. Therefore, metasomatism is the best to explain the non-CHARC character induced by an alkaline solution. Primary Mg-Ca-bearing amphiboles (e.g., magneso-arvedsonite) in the Gebel El Bakriyah highly fractionated younger granite are in favor of igneous conditions but some secondary amphiboles enriched in Fe, Na, and K (e.g., ferrobarrosite) indicates a metasomatic origin.

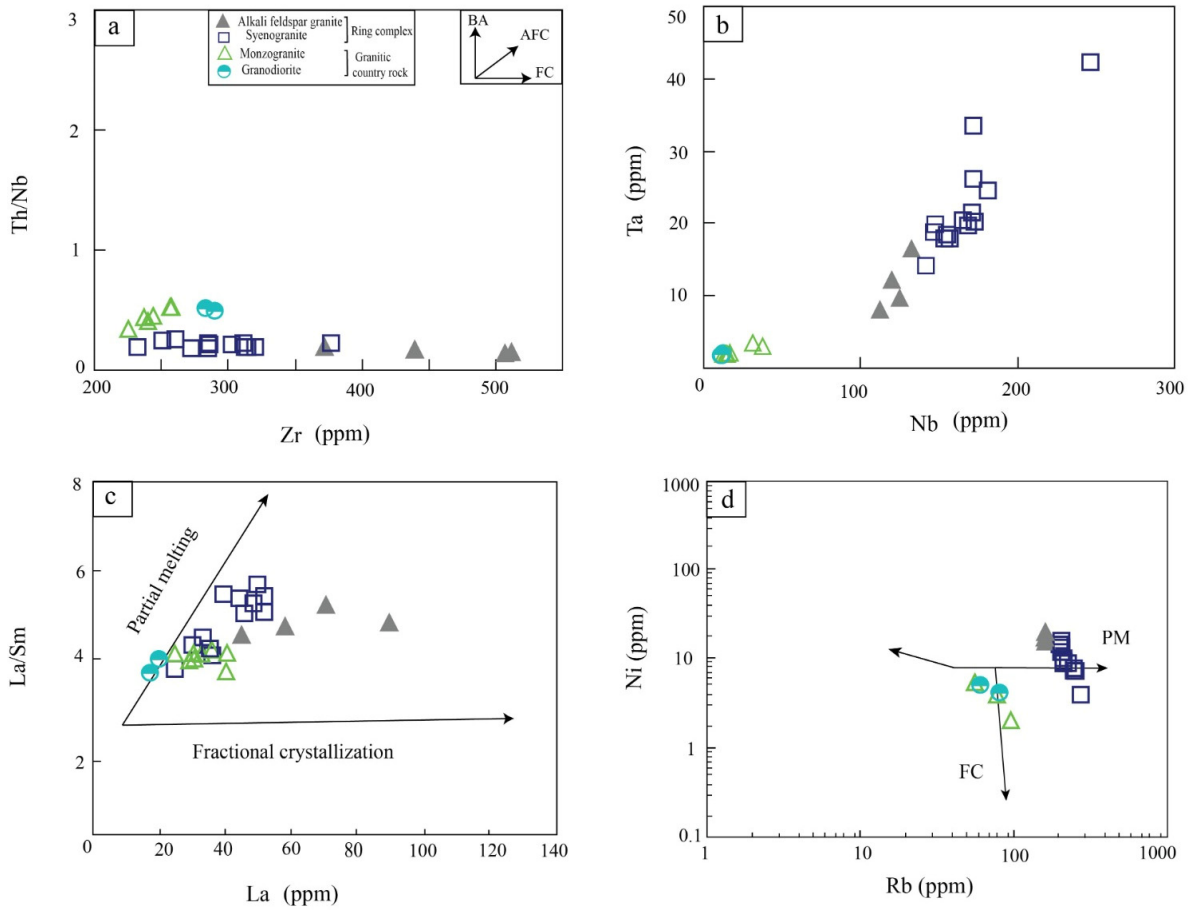

Figure 8. (**a**) Fractional crystallization (FC) and lesser assimilation assignment for the Gebel El-Bakriyah A-type granites based on the Zr vs. Th/Nb diagram [65]. (**b**) Positive correlation of Nb vs. Ta contents as an indicator of fractional crystallization in felsic magma. (**c**) Plots of La vs. La/Sm ratio indicating two processes: namely the partial melting and fractional crystallization for the studied granites (after [66]). (**d**) Ni vs. Rb compositional variation diagram showing fractional crystallization and partial melting trends of the studied granites [67]. (Abbreviations of crystallization trends: FC = Fractional crystallization, AFC = Assimilation-Fractional Crystallization, and BA = Bulk Assimilation (BA).

7.4. Mineralogical Constraints for Petrogenesis

7.4.1. Biotite and Apatite

Fe- and Mg-biotite in the investigated A-type granite are exclusively primary and formed in a proper magmatic condition. None of our biotite analyses plots in the field of re-equilibrated indicating negligible recrystallization during the late magmatic stage [35]. Primary biotite in the Gebel El-Bakriyah A-type granites support the calc-alkaline to alkaline magma sources for the monzogranite country rocks and the two zones of the BRC, respectively (Figure 6c). Content of Ti and the ratio of $Mg/(Mg + Fe^{2+})$ are very sensitive to crystallization temperature in felsic magmas (e.g., [68]. Plots of biotite analyses from the Gebel El-Bakriyah A-type granites on the binary diagram of [68] suggest their crystallization at a temperature between 600 and 700 °C (Figure 9c).

Apatite is essentially a Ca-phosphate mineral that forms in all kinds of rocks in the earth's crust and has a unique structure containing traces of Na, Sr, Fe, Mn, U, Th, Y, and REEs, as well as halogens (F, Cl) and hydroxyl group [69,70]. It is an important accessory mineral in magmatic rocks, which can be used as a petrogenetic indicator in magmatic and hydrothermal systems [71]. On the classification diagram of apatite designed by [72], the majority of apatite analyses from the Gebel El-Bakriyah A-type granite are magmatic (Figure 9d). In addition, apatite is useful to trace the history of magmatic differentiation based on its contents of Mg and Mn [73,74]. According to [74], Mg content in apatite increases proportionally to its concentration in the felsic magma, particularly peraluminous, during magmatic differentiation together with a considerable rise in the Mn content too. Also, the rise of the Mg content in apatite enhances the rate of its crystallization [75].

7.4.2. Nb-Ta Oxides, Zircon, and REEs

In several shield rocks from different ages in the world, some accessory minerals in granitic rocks are very significant petrogenetic indicators, e.g., zircon, Nb-Ta oxides, REE-bearing minerals [76,77]. In nature, particularly the felsic intrusives (e.g., granite and pegmatite), Nb-Ta oxide ore minerals can be found including the columbite-tantalite (Mn, Fe)Nb_2O_6 to (Mn, Fe)Ta_2O_6 series, the microlite-pyrochlore (Na, Ca)$_2Ta_2O_6$(O, OH, F] to (Na, Ca)$_2Nb_2O_6$(O, OH, F) series, and wodginite [Mn(Sn, Ta, Ti)Ta_2O_8] groups [34]. The post-collisional granites in the ANS host some significant concentrations of Nb and Ta [9,78]. Based on our Whole-rock analyses for the Gebel El-Bakriyah highly fractionated granites (Table 1), the concentration of Nb in the BRC ranges from 112.6 to 172.3 ppm and in the country rocks from 7.6–19.2 ppm while the concentration of Ta in the BRC is (8–26.1 ppm) and in the country rocks between (0.05 to 0.4 ppm). The rare-metal granites from the Egyptian Eastern Desert are presumably mica- and Mn-rich [5], which is the case of the investigated BRC that bears Mn-columbite and Mn-tantalite. Zircon is an abundant accessory mineral in granitic rocks which are resistant to weathering processes [76,77]. Neither morphology nor chemical composition of zircon from the Gebel El-Bakriyah younger granites indicates a hydrothermal origin and it is typically magmatic. As we previously mentioned, the whole-rock content of Zr in the BRC and its granitic country rock (averages = 356 ppm and 253 ppm, respectively) are exclusive for proper magmatic condition (T = 816–905 °C, Table 1) based on the calculation of Zr saturation [44,71].

Alkali feldspar granite is characterized by high abundance REE (∑REE = 358–547) than syenogranite (∑REE = 159–285), monzogranite (∑REE = 102–105), and granodiorite (∑REE = 103–119). Syenogranite has enrichment in LREE to HREE (Lan/Lun) = 18.2–39 than alkali feldspar granite (Lan/Lun) = 17.3–22.2 and monzogranite has (Lan/Lun) = 8.02–10.7 and in granodiorite has slightly enrichment in LREE to HREE (Lan/Lun) = 4.2. Eu/Eu* in the investigated granites = 4.03–4.2 except granodiorite Eu/Eu*= 0.27–0.88, which is a function of extensive fractionation of feldspars by magmatic differentiation that stabilizes Eu as Eu^{2+} in reducing condition [79,80]. We present whole-rock analyses (Table 1), which show enrichment of La, Ce, Pr, and Nd in granites constituting the BRC compared with the granitic country rocks. The Tetrad effect (TE) of REEs during the late magmatic stage is meaningful though it is not present in all granites, the ones enriched in fluid-mobile

elements such as Li, B, and halogens like F and Cl [81]. The phenomenon of the tetrad effect in the REEs patterns of granite helps to trace either fractional crystallization during differentiation or the interplay of coexisting magma-fluid systems in the late stage of crystallization [82] and this tetrad effect is seen in Figure 9e. We believe that F, evidenced by the presence of interstitial fluorite, plays an important role in the enrichment of REEs in the Gebel El-Bakriyah younger granites. In highly fractionated granites, F influences the enrichment of REEs and HFSE in the form of fluorine-based complexes as the element remains dissolved in the magma until fractionation is ceased and fluorite fills the interstitial spaces in granite [83,84] or forms independent fluorite veins which the case of the Gebel El-Bakriyah area.

7.4.3. Fe-Ti Oxides and Chlorite

Homogeneous Fe-Ti oxides, particularly ilmenite, in the Gebel El Bakriyah A-type granites, alter to secondary titanite in the form of a continuous reaction rim (Figure 3e). From the petrogenetic point of view, this secondary titanite, as well as the sub-graphic rutile-hematite intergrowths after ilmenite, are indicators of late stage deuteric alterations. Mafic and felsic arc-related and post-collisional intrusions in the ANS contain Mn-bearing ilmenite in which Mn increases with the progress of magmatic differentiation [85]. Ilmenite from the Gebel El-Bakriyah A-type granite is Mg-poor (MgO as much as 0.05 wt%) whereas MnO content reaches up to 9.8 wt%. This high Mn content is consistent with the evolution of highly fractionated A-type granites, and the BRC syenogranite and alkali feldspar granite in particular.

Chlorite-group minerals occur as secondary phases, which pseudomorph magmatic biotite. The chemistry of this chlorite is sensitive to temperature and hence the temperature of late stage deuteric alteration can be estimated. In the chlorite structure, occupancy and substitution of Fe, Mg, and Al in the tetrahedral and octahedral sites are common [86,87]. The available chlorite analyses in the Gebel El Bakriyah granitic rocks were possible from the monzogranite country rock and indicate a diabanite composition (Figure 7e). Based on the percentage of Al and its portioning among the octahedral and tetrahedral sites, we used the chlorite geothermometer formulated by [88] to estimate the temperature of alteration numerically. Geothermometric calculations for chlorite in the Gebel El-Bakriyah monzogranite yielded a deuteric alteration temperature of 442 °C.

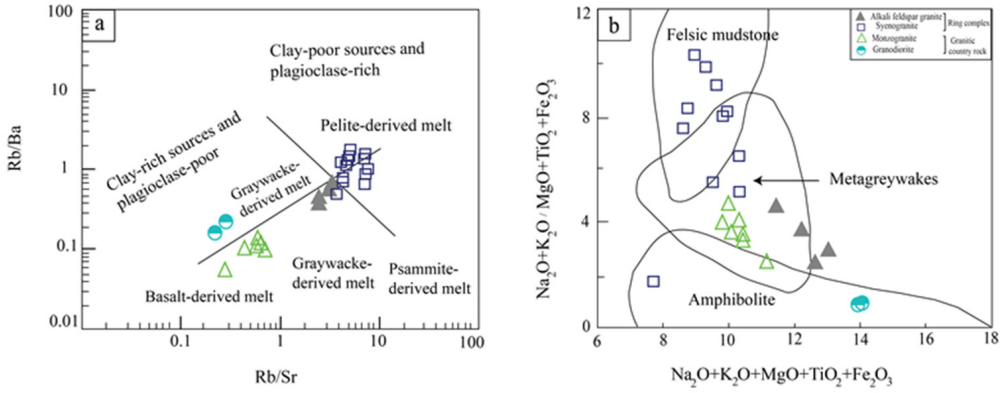

Figure 9. *Cont.*

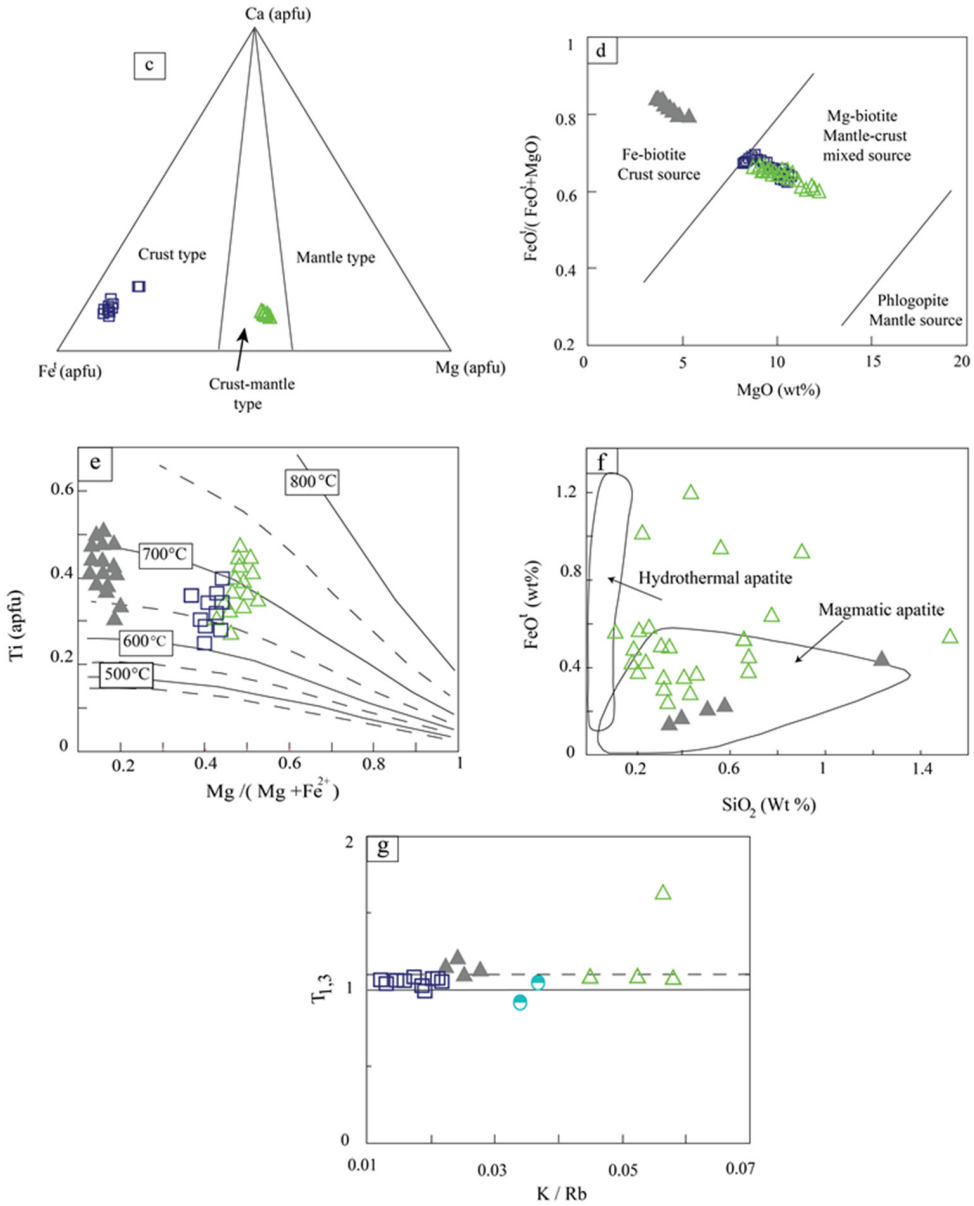

Figure 9. (**a**) Rb/Ba vs. Rb/Sr for the studied granites [62]. (**b**) The compositions of the studied granitic rocks, compared to compositional ranges of various experimental metasediment- and amphibolite-derived melts [89]. (**c**) Crust and mixed crust-mantle source of the Gebel El Bakriyah A-type granite based on amphibole chemistry [90]. (**d**) Crystallization of Mg-biotite and Fe-biotite from mixed crust-mantle and crust source for the monzogranite + syenogranite and alkali feldspar granite, respectively [91]. (**e**) The crystallization temperature of biotite in the Gebel El Bakriyah A-type granite [68]. (**f**) Magmatic origin of apatite from the investigated granites [72]. (**g**) Lanthanide tetrad effect in some granite varieties [64].

7.5. Geodynamic Model

The ANS represents one of the best examples of Precambrian (Neoproterozoic) juvenile crusts in the world [22,92]. Granitic rocks are major components in the Eastern Desert of Egypt and they represent the emplacement of different magma compositions from the oceanic spread until the post-collisional continental extension. There are several researchers who determined age of different types of granitic rocks in Egypt, particularly in the central part where Gebel El Bakriyah area is located. For example, [93] used Rb/Sr isochron to determine age of emplacement of granodiorite in the adjacent Wadi El-Miyah area, which

yielded the age 674 ± 13 Ma contemporaneous with the volcanic arc stage. Also, 614 ± 8 Ma U/Pb zircon was assigned as the age of similar granodiorite and tonalite intrusions, e.g., in Abu Ziran area. This gives an indication of wide time span of arc formation in the central Eastern Desert up to 60 Ma or alternatively there were more than arc. Some other granodiorite intrusions at the Homr Akarem and Homret Mikpid in the southern part of the Eastern Desert were emplaced at 630–620 Ma [94] and at 643 ± 9 Ma for the Um Rus tonalite-granodiorite intrusion [95], and the youngest phase (i.e., 620 Ma) was believed to represent the transition between arc to typical anorogenic setting similar to the case of Gebel El Bakriyah area [96]. On the other hand, typical anorogenic or post-colllisional A-type granite intrusions in the central Eastern Desert of Egypt, e.g., at Um Had area is assigned a U–Pb zircon age of 590–3.1 Ma [97]. Generally, felsic magmatism in the Eastern Desert that produced post-collisional A-type granites, e.g., El-Missikat, Abu Harba, and Gattar yielded single crystal zircon age of ~600 Ma [98].

Bentor [99] divided granites of the Arabian-Nubian Shield into two categories: an older syn- to late-orogenic granites (880–610 Ma), and younger post-orogenic to anorogenic granite (600–475 Ma). Ages determined for the older granites from the Egyptian Eastern Desert are less than 750 Ma [100]. The Egyptian late- to post-tectonic younger granites were formed between 600 and 550 Ma, [93] or 600 and 475 Ma [94]. On the other hand, the 635–580 Ma or 610 and 590 Ma ages are used to distinguish the emplacement of the Egyptian post collisional younger granite [101]. They have been emplaced as two separate suites, although substantially overlapping calc-alkaline and alkaline pulses at 635–590 Ma and 608–580 Ma, respectively [102]. The BRC is located in the central part of the Egyptian Eastern Desert, and it is a part of the northern segment of the Arabian-Nubian Shield that belongs to the third stage (i.e., the post-collisional) in most. And this is characterized by alkaline magmatism including A-type granites. According to [103], a Rb-Sr isochron assigned 520–506 Ma age of Gebel El Bakriyah granites, particularly the BRC.

The younger granites in the Gebel El Bakriyah area formed during the post-collisional stage, i.e., emplacement was controlled by within-plate tectonics in which lithospheric delamination took place to generate mafic and felsic magma batches [24]. Based on our present field and laboratory data, we assume that the formation of the Gondwana assembly during the last stage of subduction (Figure 10a) marked the beginning of the collisional phase, which is marked the first stage of the evolution of El Bakriyah granites represented by granodiorite country rock. This is resulted by the dehydration of the subducted plate comparatively at low pressure, which made it easier for the upper mantle to melt and penetrate the continental crust, forming calc-alkaline volcanic arc magma. The orogenic activity peaked as a result of the water supply being cut off during the transitional period that started when subduction reached its warning stage. This phase denotes the post-orogenic transition from the calc-alkaline to the alkaline stage, despite the anorogenic regime being relaxed and represented by the evolution of monzogranite rocks. We believe that the BRC resulted from decompression melting of crustal source material followed by break-off and delamination of the lithosphere, which was accepted for vast areas in the Eastern Desert of Egypt (e.g., [104]). Mafic melts were produced by melting the residual lithosphere by high heat flux during the transition from the compressional to the extensional phase, and the lithospheric delamination played a significant part in this evolution. The final stage of the evolution of the Gebel El Bakriyah granites is the post-collisional within-plate stage (Figure 10b). When magma from the mantle ascended along the fractured crust during tension and relaxation periods. It causes a relatively greater supply of crustal alkaline magmas to partially melt, which is represented by two successive evolution of syenogranite and alkali feldspar granite.

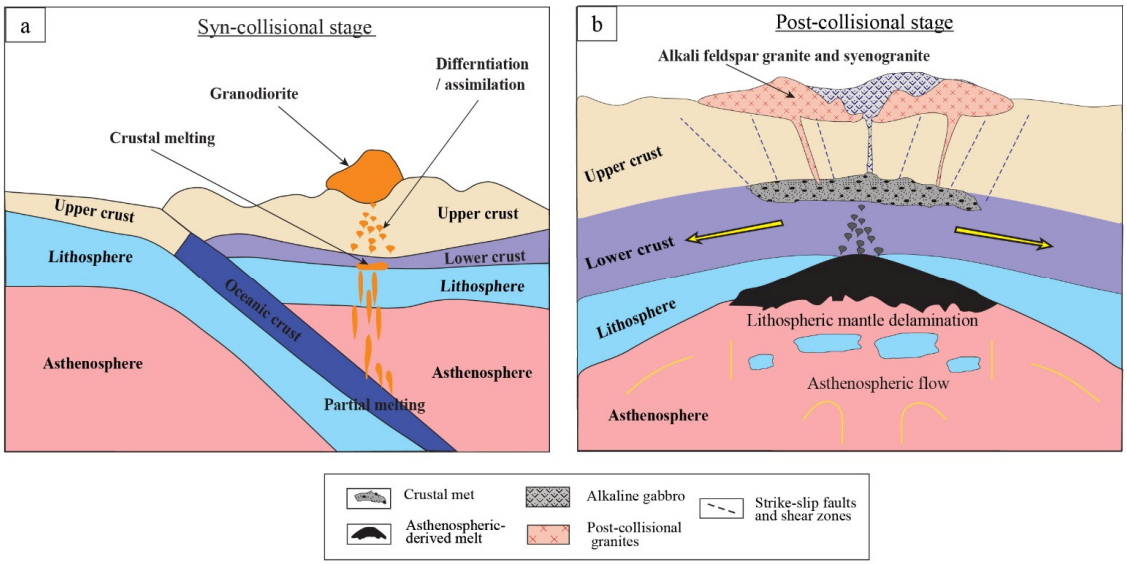

Figure 10. A suggested geodynamic model for the generation of A-type magma by dehydration melting of lithospheric delamination in an extensional tectonic regime during the Late Neoproterozoic in the Arabian-Nubian Shield (ANS). The Gebel El Bakriyah complex witnessed two successive post-collisional magmatic episodes, the first is mafic that formed the younger gabbros [24] and the A-type granites (present study).

Our geochemical data are in favor of progressive magmatic differentiation, fractionation, and little assimilation to form the Gebel El Bakriyah A-type younger granites along the fracture system and this extends to a proper anorogenic/within-plate environment. Other parts in the ANS have A-type younger granites that experienced high fractionation, mostly from a metasedimentary source rock and not tonalite, which is the case of the BRC. Therefore, it is believed that the fractures of the extensional tectonics were shear zones that facilitated the upwelling of two independent suites of calc-alkaline and alkaline felsic magmatism. Similar models have been proposed for the generation of A-type granites in the ANS either in the form of ring complexes or not e.g., [5,13]. A-type younger granites formed as post-collisional derivatives of the delaminated mantle in extensional tectonics form similar ring complexes, e.g., those at Jabal Al-Hassir [93] and Jabal Aja [4] in the Arabian Shield of Saudi Arabia. These ring complexes are parts of Caulderon subsidence structures and calderas above the felsic plutons in the western Arabian Peninsula (i.e., the eastern segment of ANS), and represent the transition from convergent to extensional tectonics [105].

Mineralogy and geochemistry of the Gebel El Bakriyah younger granites provide some evidence for F-and Ba-rich fluids during the late stage of felsic magma fractionation. Interstitial fluorite and fluorite veins are strong evidence for F and Ba enrichment in the felsic injection of dominating alkaline composition in the post-collisional environment at high temperature as low as 830 °C [44,83]. Fluorite in similar A-type granites from the ANS (e.g., [106,107] and others) confirm our observations and conclusion that the F-complexes of REEs, U, and Th, are very characteristic for the highly fractionated granites like the case of Gebel El Bakriyah younger A-type granites. Finally, A-type younger granites in the entire ANS form by delamination of the lithospheric lower crust in different ages that can be as old as Cryogenian (e.g., 686 Ma; [105] or Ediacaran (e.g., 634 Ma to 580 Ma; [92]) or down to 550 Ma [21]. Gebel El Bakriyah A-type granites are peculiar Ediacaran intrusions, which are formed by high-T melting from a crustal source (Cryogenian crust, possibly Tonian too) that fractionated during upwelling along fault planes/shear zone in a typical extensional regime of the Neoproterozoic post-collisional phase of the ANS evolution. The Gebel El Bakriyah A-type granites are equivalent to other calc-alkaline peraluminous granites in the ANS (e.g., [4,21]. In other shield terranes of Neoproterozoic age similar to

the ANS, e.g., the Brasiliano, A-type magmatism at ~630 Ma ago is comparable to the Gebel El Bakriyah case. Recycled/reworked ancient oceanic and arc-related crustal materials in the asthenosphere leads to the formation of alkaline magmatism [108–111], and hence it is a potential source of upwelling melt to form A-type granites in a proper post-collisional extension, i.e., within-plate.

8. Conclusions

(1) The Gebel El Bakriyah younger granites comprise a prominent ring complex (BRC) consisting of syenogranite core and alkali feldspar rim. These two granite varieties pertain to typical A-type characteristics. The ring complex was emplaced in a within-plate setting whereas the monzogranite represents a transition between the arc and anorogenic settings.

(2) A calc-alkaline composition is assigned for the three younger granite varieties. All of them have the high-K signature of peraluminous melts that were emplaced in the form of their independent pulses, one produced the monzogranite country rocks and two successive ones formed the syenogranite and alkali feldspar granite, respectively.

(3) The three varieties of younger granites of Ediacaran age in the Gebel El Bakriyah area show enrichment of rare metals (Mn-rich columbite-tantalite), F and Fe, i.e., ferroan granites, which are highly fractionated. This resulted in frequent interstitial fluorite in the granites as well as the formation of excavated fluorite-rich quartz veins.

(4) From the geodynamic point of view, the Gebel El Bakriyah younger granites formed by high-T dehydration melting of a mixed crust-mantle source dominated by metasediments and amphibolite, i.e., delamination of the lithospheric crust. This is followed by high fractionation and upwelling of three independent felsic magma pulses along faults in an extensional tectonic regime.

(5) The BRC and its monzogranite country rocks are peculiar examples of Neoproterozoic (Ediacaran) post-collisional magmatism comparable to those in other Precambrian Shields in the world.

(6) Although most of the fluorite and barite veins are excavated, there are still more exploration efforts that must be carried out to maximize the potentiality of critical materials in the area, including the Nb-Ta resources.

Supplementary Materials: The following supporting information can be downloaded at: https://www.mdpi.com/article/10.3390/min13101273/s1, Supplementary File S1: Whole rock geochemistry and mineral chemistry data [112].

Author Contributions: Conceptualization, A.A.A.E.-F., A.A.S. and A.A.M.; methodology, A.A.A.E.-F.; software, A.A.A.E.-F.; validation, A.A.A.E.-F., A.A.S., M.K.A. and A.A.M.; formal analysis, A.A.A.E.-F. and M.K.A.; investigation, A.A.A.E.-F., A.A.S., M.K.A. and A.A.M.; resources, A.A.A.E.-F.; data curation, A.A.A.E.-F. and A.A.S.; writing—original draft preparation, A.A.A.E.-F.; writing—review and editing, A.A.A.E.-F., A.A.S. and A.A.M.; visualization, A.A.S. and A.A.M.; supervision, A.A.S., M.K.A. and A.A.M.; project administration, A.A.S.; funding acquisition, M.K.A. All authors have read and agreed to the published version of the manuscript.

Funding: Internal Project No. 13010312 of The National Research Centre of Egypt entitled "Evaluation of alkaline ring complexes as a potential source of some strategic mineralization".

Data Availability Statement: Data are available upon request to the corresponding author.

Acknowledgments: The present paper is part of MSc Thesis submitted by the first author to the Faculty of Science, Cairo University. The authors would like to thank Cairo University for the logistics, which enabled us to have field trips and preparation of thin-, polished- and polished-thin sections and pulverization of samples for chemical analyses. Hesham Mokhtar is acknowledged for his patience and sincere revision during the preparation of the manuscript. We also thank Abdallah Atef for his assistance in the field. We would like to thank the editor and three anonymous reviewers for their patience and very fruitful discussion that improved quality of the paper.

Conflicts of Interest: The authors declare no conflict of interest.

References

1. El-Bialy, M.Z.; Omar, M.M. Spatial association of Neoproterozoic continental arc I-type and post-collision A-type granitoids in the Arabian-Nubian Shield: The Wadi Al-Baroud older and younger granites, North Eastern Desert, Egypt. *J. Afr. Earth Sci.* **2015**, *103*, 1–29. [CrossRef]
2. El-Bialy, M.Z. Precambrian Basement Complex of Egypt. In *The Geology of Egypt*; Regional Geology Reviews; Hamimi, Z., El-Barkooky, A., Martínez Frías, J., Fritz, H., Abd El-Rahman, Y., Eds.; Springer: Cham, Switzerland, 2020; pp. 37–79.
3. Abd El-Naby, H.H. The Egyptian granitoids: An up-to-date synopsis. In *Geology of the Egyptian Nubian Shield*; Regional Geology Reviews; Hamimi, Z., Arai, S., Fowler, A.R., El-Bialy, M.Z., Eds.; Springer: Cham, Switzerland, 2021; pp. 239–265.
4. Abuamarah, B.A. Genesis and petrology of post-collisional rare-metal-bearing granites in the Arabian Shield: A case study of Aja ring complex, northern Saudi Arabia. *J. Geol.* **2020**, *128*, 131–156. [CrossRef]
5. Moussa, H.E.; Asimow, P.D.; Azer, M.K.; Maaty, M.A.A.; Adel, I.M.; Yanni, N.N.; Mubarak, H.S.; Wilner, M.J.; Elsagheer, M.A. Magmatic and hydrothermal evolution of highly fractionated rare-metal granites at Gabal Nuweibi, Eastern Desert, Egypt. *Lithos* **2021**, *400–401*, 106405. [CrossRef]
6. Hassaan, M.M.; Desoky, E.H. Granites in the tectonic environs of the Nubian Shield, Egypt: Geochemical characterization and new contributions. *Curr. Res. Earth Sci.* **2016**, *10*, 59–103.
7. Lundmark, A.M.; Andresen, A.; Hassan, A.; Augland, L.E.; Abu El-Rus, M.A.; Boghdady, G.Y. Repeated magmatic pulses in the East African Orogen of Central Eastern Desert, Egypt: An old idea supported by new evidence. *Gondwana Res.* **2012**, *22*, 227–237. [CrossRef]
8. Hargrove, U.S.; Stern, R.J.; Griffin, W.R.; Johnson, P.R.; Abdelsalam, M.G. From island arc to craton: Timescales of crustal formation along the Neoproterozoic Bir Umq Suture zone, Kingdom of Saudi Arabia. In *Saudi Geological Survey*; Technical Report SGS-TR; Saudi Geological Survey: Jeddah, Saudi Arabia, 2006; 69p.
9. Azer, M.K.; Abdelfadil, K.M.; Asimow, P.D.; Khalil, A.E. Tracking the transition from subduction-related to post-collisional magmatism in the north Arabian–Nubian Shield: A case study from the Homrit Waggat area of the Eastern Desert of Egypt. *Geol. J.* **2020**, *55*, 4426–4452. [CrossRef]
10. Eby, G.N. Chemical subdivisions of the A-type granitoids: Petrogenesis and tectonic implications. *Geology* **1992**, *20*, 641–644. [CrossRef]
11. Robinson, F.A.; Bonin, B.; Pease, V.; Anderson, J.L. A discussion on the tectonic implications of Ediacaran late- to post-orogenic A-type granite in the northeastern Arabian Shield, Saudi Arabia. *Tectonics* **2017**, *36*, 582–600. [CrossRef]
12. Heikal, M.T.S.; Khedr, M.Z.; El-Monesf, M.A.; Gomaa, S.R. Petrogenesis and geodynamic evolution of Neoproterozoic Abu Dabbab albite Granite, Central Eastern Desert of Egypt: Petrological and geochemical constraints. *J. Afr. Earth Sci.* **2019**, *158*, 103518. [CrossRef]
13. Abuamarah, B.A.; Azer, M.K.; Seddik, A.M.A.; Asimow, P.D.; Guzman, P.; Fultz, B.T.; Wilner, M.J.; Dalleska, N.; Darwish, M.H. Magmatic and post-magmatic evolution of post-collisional rare-metal bearing granite: The Neoproterozoic Homrit Akarem granitic intrusion, southeastern Desert of Egypt, Arabian-Nubian shield. *Geochemistry* **2022**, *82*, 125840. [CrossRef]
14. Sami, M.; Ntaflos, T.; Farahat, E.S.; Mohamed, H.A.; Hauzenberger, C.; Ahmed, A.F. Petrogenesis and geodynamic implications of Ediacaran highly fractionated A-type granitoids in the north Arabian-Nubian Shield (Egypt): Constraints from whole-rock geochemistry and Sr-Nd isotopes. *Lithos* **2018**, *304–307*, 329–346. [CrossRef]
15. Loiselle, M.; Wones, D. Characteristics and origin of anorogenic granites. In *Abstracts with Programs*; Geological Society of America: Boulder, CO, USA, 1979; Volume 11, p. 468.
16. Moreno, J.A.; Montero, P.; Abu Anbar, M.; Molina, J.F.; Scarrow, J.H.; Talavera, C.; Cambeses, A.; Bea, F. SHRIMP U-Pb zircon dating of the Katerina ring complex: Insights into the temporal sequence of Ediacaran calc-alkaline to per-alkaline magmatism in southern Sinai, Egypt. *Gond. Res.* **2012**, *12*, 887–900. [CrossRef]
17. Mahmoud, M.S. Geological and Geochemical Studies on the Rocks of Gebel El-Hisinat Area, Central Eastern Desert, Egypt. Master's Thesis, Assuit University, Assuit, Egypt, 1984; 109p.
18. El-Sayed, M.M.; Mohamed, F.H.; Furnes, H. Petrological and geochemical constraints on the evolution of late Pan-African Bakriya post-orogenic ring complex, Central Eastern Desert, Egypt. *Neues Jahrb. Mineral. Ab-Handl.* **2004**, *180*, 1–32. [CrossRef]
19. Saleeb-Roufaiel, G.S.; Samuel, M.D.; Hilmy, M.E.; Moussa, H.E. Fluorite mineralization at El-Bakriya, Eastern Desert of Egypt, Egypt. *J. Geol.* **1982**, *26*, 9–18.
20. Eyal, M.; Litvinovsky, B.; Jahn, B.M.; Zanvilevich, A.; Katzir, Y. Origin and evolution of post-collisional magmatism: Coeval Neoproterozoic calc-alkaline and alkaline suites of the Sinai Peninsula. *Chem. Geol.* **2010**, *269*, 153–179. [CrossRef]
21. Be'eri-Shlevin, Y.; Samuel, M.D.; Azer, M.K.; Rämö, O.T.; Whitehouse, M.J.; Moussa, H.E. The late Neoproterozoic Ferani and Rutig volcano-sedimentary successions of the northernmost Arabian–Nubian Shield (ANS): New insights from zircon U-Pb geochronology, geochemistry and O–Nd isotope ratios. *Precambrian Res.* **2011**, *188*, 21–44. [CrossRef]
22. Stern, R.J. Arc assembly and continental collision in the Neoproterozoic East African Orogen: Implications for the consolidation of Gondwanaland. *Annu. Rev. Earth Planet. Sci.* **1994**, *22*, 319–351. [CrossRef]
23. Abdelnasser, A. Genesis of the Gold Mineralization at Atud Area, Central Eastern Desert of Egypt: Geological, Ore Mineralogical and Geochemical Approaches. Ph.D. Thesis, Istanbul Technical University, Istanbul, Turkey, 2016.

24. Azer, M.K.; Surour, A.A.; Madani, A.A.; Ren, M.; Abd El-Fatah, A.A. Mineralogical and geochemical constraints on the post-collisional mafic magmatism in the Arabian-Nubian Shield: An example from the El-Bakriya Area, Central Eastern Desert, Egypt. *J Geol.* **2022**, *130*, 209–230. [CrossRef]
25. Abd El-Fatah, A.A.; Surour, A.A.; Madani, A.A.; Azer, M.K. Integration of Landsat-8 and reflectance spectroscopy data for the mapping of Late Neoproterozoic igneous ring complexes in an arid environment: A case study of the Gebel El-Bakriyah area, Eastern Desert, Egypt. *J. Min. Environ.* **2023**, *14*, 13–31.
26. El-Amin, H. Radiometric and Geological Investigations of El Bakriya Area, Eastern Desert, Egypt. Ph.D. Thesis, Cairo University, Cairo, Egypt, 1975; 224p.
27. Bence, A.E.; Albee, A.L. Empirical correction factors for the electron microanalysis of silicates and oxides. *J. Geol.* **1968**, *76*, 382–403. [CrossRef]
28. Middlemost, E.A.K. Magmas and magmatic rocks: An introduction to igneous petrology. *Geol. Mag.* **1985**, *123*, 87–88.
29. Streckeisen, A. Each plutonic rock has its proper name. *Earth-Sci. Rev.* **1976**, *12*, 1–33. [CrossRef]
30. Maniar, P.D.; Piccoli, P.M. Tectonic discrimination of granitoids. *Geol. Soc. Am. Bull.* **1989**, *101*, 635–643. [CrossRef]
31. Evensen, N.M.; Hamilton, P.J.; Onions, R.K. Rare-earth abundances in chondritic meteorites. *Geochim. Cosmochim. Acta* **1978**, *42*, 1199–1212. [CrossRef]
32. Sun, S.S.; McDonough, W.E. Chemical and isotopic systematics of oceanic basalts: Implications for mantle composition processes. In *Magmatism in the Ocean Basins. Geological Society*; Saunders, A.D., Norry, M.J., Eds.; Special Publications: London, UK, 1989; pp. 313–345.
33. Richard, L.R. *MinPet: Mineralogical and Petrological Data Processing System*, version 2.02; MinPet Geological Software: Québec, QC, Canada, 1995.
34. Deer, W.A.; Howie, R.A.; Zussman, J. *An Introduction to Rock-Forming Minerals*, 2nd ed.; Longman: Harlow, UK, 1992; 696p.
35. Deer, W.A.; Howie, R.A.; Zussman, J. *An Introduction to the Rock-Forming Minerals*, 1st ed.; Longman Scientific and Technical Publishing: Harlow, UK, 1966; 528p.
36. Nachit, H.; Ibhi, A.; Ohoud, M.B. Discrimination between primary magmatic biotites, re-equilibrated biotites, and neoformed biotites. *Comptes Rendus Geosci.* **2005**, *337*, 1415–1420. [CrossRef]
37. Leak, B.E.; Woolley, A.R.; Arps, C.E.S.; Birch, W.D.; Gilbert, M.C.; Grice, J.D.; Hawthorne, F.C.; Kato, A.; Kisch, H.J.; Krivovichev, V.G.; et al. Nomenclature of Amphiboles: Report of the sub-committee on amphiboles of the international mineralogical association, Commission on new minerals and mineral names. *Mineral. Mag.* **1997**, *61*, 295–310. [CrossRef]
38. Hey, M.H. A new review of chlorites. *Mineral. Mag.* **1954**, *30*, 277–292. [CrossRef]
39. Basak, A.; Goswami, B. The physico-chemical conditions of crystallization of the Grenvillian arfvedsonite granite of Dimra Pahar, Hazaribagh, India: Constraints on possible source regions. *Mineral. Petrol.* **2020**, *114*, 329–356. [CrossRef]
40. Watson, E.B.; Harrison, T.M. Zircon saturation revisited: Temperature and composition effects in a variety of crustal magma types. *Earth Planet. Sci. Lett.* **1983**, *64*, 295–304. [CrossRef]
41. Machev, P.; Klain, L.; Hecht, L. Mineralogy and geochemistry of biotites from the Belogradchik pluton—Some petrological implications for granitoid magmatism in north-west Bulgaria: Bulgarian Geological Society, Annual Scientific Conference of the Bulgarian Geological Society. *Geology* **2004**, *16–17*, 48–50.
42. Jayasuriya, K.D.; O'Neill, H.S.C.; Berry, A.; Campbell, S.J. A Mössbauer study of the oxidation state of Fe in silicate melts. *Am. Min.* **2004**, *89*, 1597–1609. [CrossRef]
43. Haggerty, S.E. Opaque mineral oxides in terrestrial igneous rocks. *Mineral. Soc. Am.-Short Course Notes* **1976**, *3*, 101–300.
44. King, P.L.; Chappell, B.W.; Allen, C.M.; White, A.J.R. Are A-type granites the high-temperature felsic granites? Evidence from fractionated granites of the Wangrah Suite. *Aust. J. Earth Sci.* **2010**, *48*, 501–514. [CrossRef]
45. Pearce, J.A.; Harris, N.B.W.; Tindle, A.G. Trace element discrimination diagrams for the tectonic interpretation of granitic rocks. *J. Petrol.* **1984**, *25*, 956–983. [CrossRef]
46. Chappell, B.W.; Bryant, C.J.; Wyborn, D. Peraluminous I-type granites. *Lithos* **2012**, *153*, 142–153. [CrossRef]
47. Whalen, J.B.; Frost, C. The Q-ANOR diagram: A tool for the petrogenetic and tectonomagmatic characterization of granitic suites. In Proceedings of the South-Central Section, 47th Annual Meeting, Austin, TX, USA, 4–5 April 2013; Geological Society of America: Boulder, CO, USA, 2013; Volume 7.
48. Manning, D.A.C. The effect of fluorine on liquidus phase relationships in the system Qz-Ab-Or with excess water at 1 kb. *Contrib. Mineral. Petrol.* **1981**, *76*, 206–215. [CrossRef]
49. Holtz, F.; Johannes, W.; Pichavant, M. Effect of excess aluminium on phase relations in the system Qz-Ab-Or. Experimental investigation at 2 Kbar and reduced H_2O activity. *Eur. J. Mineral.* **1992**, *4*, 137–152. [CrossRef]
50. Anderson, J.L.; Smith, D.R. The effects of temperature and fO2 on the Al-in-hornblende barometer. *Am. Mineral.* **1995**, *80*, 549–559. [CrossRef]
51. Abdel-Rahman, A.M. Nature of biotites from alkaline, calc-alkaline, and peraluminous magmas. *J. Petrol.* **1994**, *35*, 525–541. [CrossRef]
52. Frost, B.R.; Barnes, C.G.; Collins, W.J.; Arculus, R.J.; Ellis, D.J.; Frost, C.D. A geochemical classification for granitic rocks. *J. Petrol.* **2001**, *42*, 2033–2048. [CrossRef]
53. Seddik, A.M.A.; Darwish, M.H.; Azer, M.K.; Asimow, P.D. Assessment of magmatic versus post-magmatic processes in the Mueilha rare-metal granite, Eastern Desert of Egypt, Arabian-Nubian Shield. *Lithos* **2020**, *366–367*, 105542. [CrossRef]

54. Kerr, A.; Fryer, B.J. Nd isotope evidence for crust-mantle interaction in the generation of A-type granitoid suites in Labrador, Canada. *Chem. Geol.* **1993**, *104*, 39–60. [CrossRef]
55. Jarrar, G.H.; Manton, W.I.; Stern, R.J.; Zachmann, D. Late Neoproterozoic A-type granites in the northernmost Arabian-Nubian Shield formed by fractionation of basaltic melts. *Chem. Erde Geochem.* **2008**, *68*, 295–312. [CrossRef]
56. Sylvester, P.J. Post-collisional alkaline granites. *J. Geol.* **1989**, *97*, 261–280. [CrossRef]
57. Sisson, T.W.; Ratajeski, K.; Hankins, W.B.; Glazner, A.F. Voluminous granitic Desert, Egypt. *Sci. J. Fac. Sci. Minufia Univ.* **2005**, *15*, 107–129.
58. Sami, M.; Ntaflos, T.; Farahat, E.S.; Mohamed, H.A.; Ahmed, A.F.; Hauzenberger, C. Mineralogical, geochemical and Sr-Nd isotopes characteristics of fluorite-bearing granites in the Northern Arabian-Nubian Shield, Egypt: Constraints on petrogenesis and evolution of their associated rare metal mineralization. *Ore Geol. Rev.* **2017**, *88*, 1–22. [CrossRef]
59. Ballouard, C.; Poujol, M.; Boulvais, P.; Branquet, Y.; Tartèse, R.; Vigneresse, J.L. Nb-Ta fractionation in per-aluminous granites: A marker of the magmatic-hydrothermal transition. *J. Geol.* **2016**, *44*, 231–234. [CrossRef]
60. Dingwell, D.B. The structures and properties of fluorine-rich magmas: A review of experimental studies. *Can. Inst. Min. Metall. Pet.* **1988**, *39*, 1–12.
61. Wang, R.C.; Wu, F.Y.; Xie, L.; Liu, X.C.; Wang, J.M.; Yang, L.; Lai, W.; Liu, C. A preliminary study of rare-metal mineralization in the Himalayan leucogranite belts, South Tibet. *Sci. China Earth Sci.* **2017**, *60*, 1655–1663. [CrossRef]
62. Chappell, B.W. Aluminium saturation in I-and S-type granites and the characterization of fractionated haplogranites. *Lithos* **1999**, *46*, 535–551. [CrossRef]
63. Khalil, A.E.S.; Obeid, M.A.; Azer, M.K.; Asimow, P.D. Geochemistry and petrogenesis of post-collisional alkaline and peralkaline granites of the Arabian-Nubian Shield: A case study from the southern tip of the Sinai Peninsula, Egypt. *Int. Geol. Rev.* **2018**, *60*, 998–1018. [CrossRef]
64. Irber, W.; Förster, H.J.; Hecht, L.; Möller, P.; Morteani, G. Experimental, geochemical, mineralogical and O-isotope constraints on the late-magmatic history of the Fichtelgebirge granites (Germany). *Int. J. Earth Sci.* **1997**, *86*, 110–124. [CrossRef]
65. Nicolae, I.; Saccani, E. Petrology and geochemistry of the Late Jurassic calc-alkaline series associated to Middle Jurassic ophiolites in the South Apuseni Mountains (Romania). *Swiss J. Geosci.* **2003**, *83*, 81–96.
66. De Souza, Z.S.; Martin, H.; Peucat, J.J.; Jardim de Sá, E.F.; de Freitas Macedo, M.H. Calc Alkaline Magmatism at the Archean-Proterozoic Transition: The Caicoó Complex Basement (NE Brazil). *J. Petrol.* **2007**, *48*, 2149–2185. [CrossRef]
67. Schiano, P.; Monzier, M.; Eissen, J.P. Simple mixing as the major control of the evolution of volcanic suites in the Ecuadorian Andes. *Contrib. Mineral. Petrol.* **2010**, *160*, 297–312. [CrossRef]
68. Henry, D.J.; Guidotti, C.V.; Thomson, J.A. The Ti-saturation surface for low- to medium-pressure metapelitic biotites: Implications for geothermometry and Ti-substitution mechanisms. *Am. Min.* **2005**, *90*, 316–328. [CrossRef]
69. Piccoli, P.M.; Candela, P.A. Apatite in igneous systems. In *Phosphates: Geochemical, Geobiological, and Materials Importance*; Reviews in Mineralogy and Geochemistry; GeoScienceWorld: McLean, VA, USA, 2002; Volume 48, pp. 255–292.
70. Webster, J.D.; Piccoli, P.M. Magmatic apatite: A powerful, yet deceptive, mineral. *Elements* **2015**, *11*, 177–182. [CrossRef]
71. Zeng, L.P.; Li, X.F.; Hu, H.; McFarlane, C. In situ elemental and isotopic analysis of fluorapatite from the Taocun magnetite-apatite deposit, Eastern China: Constraints on fluid metasomatism. *Am. Min.* **2016**, *101*, 2468–2483. [CrossRef]
72. Chen, L.; Yan, Z.; Wang, Z.Q.; Wang, K. Characteristics of Apatite from 160–140 Ma Cu (Mo) and Mo (W) Deposits in East Qinling. *Geol. Acta* **2017**, *91*, 1925–1941.
73. Miles, A.J.; Graham, C.M.; Hawkesworth, C.J.; Gillespie, M.R.; Hinton, R.W.; Bromiley, G.D. Apatite: A new redox proxy for silicic magmas. *Geochim. Cosmochim. Acta* **2014**, *132*, 101–119. [CrossRef]
74. Nathwani, C.L.; Loader, M.A.; Wilkinson, J.J.; Buret, Y.; Sievwright, R.H.; Hollings, P. Multi-stage arc magma evolution recorded by apatite in volcanic rocks. *Geology* **2020**, *48*, 323–327. [CrossRef]
75. Prowatke, S.; Klemme, S. Trace element partitioning between apatite and silicate melts. *Geochim. Cosmochim. Acta* **2006**, *70*, 4513–4527. [CrossRef]
76. Hoskin, P.W.O.; Schaltegger, U. The composition of zircon and igneous and metamorphic petrogenesis. *Rev. Mineral. Geochem.* **2003**, *53*, 27–62. [CrossRef]
77. Erdmann, S.; Wodicka, N.; Jackson, S.E.; Corrigan, D. Zircon textures and composition refractory recorders of magmatic volatile evolution. *Contrib. Mineral. Petrol.* **2013**, *165*, 45–71. [CrossRef]
78. Abuamarah, B.A.; Azer, M.K.; Asimow, P.D.; Shi, Q. Petrogenesis of the post-collisional rare-metal-bearing Ad-Dayheen granite intrusion, Central Arabian Shield. *Lithos* **2019**, *384–385*, 105956. [CrossRef]
79. McKay, G.A. Partitioning of rare earth elements between major silicate minerals and basaltic melts. In *Geochemistry and Mineralogy of Rare Earth Elements*; Lipin, B.R., McKay, G.A., Eds.; De Gruyter: Berlin, Germany; Boston, MA, USA, 1989; pp. 45–78.
80. Lee, S.G.; Asahara, Y.; Tanaka, T.; Lee, S.R.; Lee, T. Geochemical significance of the Rb-Sr, La-Ce, and Sm-Nd isotope systems in A-type rocks with REE tetrad patterns and negative Eu and Ce anomalies: The Cretaceous Muamsa and Weolaksan granites, South Korea. *Geochemistry* **2013**, *73*, 75–88. [CrossRef]
81. London, D. The application of experimental petrology to the genesis and crystallization of granitic pegmatites. *Can. Mineral.* **1992**, *30*, 499–540.

82. Monecke, T.; Kempe, U.; Monecke, J.; Sala, M.; Wolf, D. Tetrad effect in rare earth element distribution patterns: A method of quantification with application to rock and mineral samples from granite-related rare metal deposits. *Geochim. Cosmochim. Acta* **2002**, *66*, 1185–1196. [CrossRef]
83. Abdel-Rahman, A.M.; El-Kibbi, M.M. Anorogenic magmatism: Chemical evolution of the Mount El-Sibai A-type complex (Egypt), and implications for the origin of within-plate felsic magmas. *Geol. Mag.* **2001**, *138*, 67–85. [CrossRef]
84. Agangi, A.; Kamenetsky, V.S.; McPhie, J. The role of fluorine in the concentration and transport of lithophile trace elements in felsic magmas: Insights from the Gawler Range Volcanics, South Australia. *Chem. Geol.* **2010**, *273*, 314–325. [CrossRef]
85. Surour, A.A.; Ahmed, A.H.; Harbi, H.M. Mineral chemistry as a tool for understanding the petrogenesis of Cryo-genian (arc-related) Ediacaran (post-collisional) gabbros in the western Arabian Shield of Saudi Arabia. *Int. J. Earth Sci.* **2017**, *106*, 1597–1617. [CrossRef]
86. Laird, J. Chlorites: Metamorphic petrology. In *Hydrous Phyllosilicates. (Exclusive of Micas)*; Reviews in Mineralogy; Bailey, S.W., Ed.; Walter de Gruyter GmbH & Co KG.: Berlin, Germany, 1988; pp. 405–453.
87. Inoue, A.; Kurokawa, K.; Hatta, T. Application of chlorite geothermometry to hydrothermal alteration in Toyoha geothermal system, Southwestern Hokkaido, Japan. *Resour. Geol.* **2010**, *160*, 52–70. [CrossRef]
88. Jowett, E.C. Fitting iron and magnesium into the hydrothermal chlorite geothermometer. In Proceedings of the GAC/MAC/SEG Joint Annual Meeting, Program with Abstracts, Toronto, ON, Canada, 27–29 May 1991; Volume 16, p. 62.
89. Patiño Douce, A.E. What do experiments tell us about relative contributions of crust and mantle to the origin of granitic magma? In *Understanding Granites: Integrating New and Classical Techniques*; Castro, A., Fernandez, C., Vigneress, J.L., Eds.; Geological Society, London, Special Publications: London, UK, 1999; Volume 168, pp. 55–75.
90. Xie, Y.W.; Zhang, Y.Q. Peculiarities and genetic significance of hornblende from granite in the Hengduansan region. *Acta Mineral. Sin.* **1990**, *10*, 35–45.
91. Zhou, Z.X. The origin of intrusive mass in Fengshandong, Hubei province. *Acta Petrol. Sin.* **1986**, *2*, 59–70.
92. Ali, K.A.; Kröner, A.; Hegner, E.; Wong, J.; Li, S.-Q.; Gahlan, H.A.; Abu El Ela, F.F. U-Pb zircon geochronology and Hf–Nd isotopic systematics of Wadi Beitan granitoid gneisses, Southeastern Desert, Egypt. *Gondwana Res.* **2015**, *27*, 811–824. [CrossRef]
93. Stern, R.J.; Hedge, C.E. Geochronologic constraints on late Precambrian crustal evolution in the Eastern Desert of Egypt. *Am. J. Sci.* **1985**, *285*, 97–127. [CrossRef]
94. Ali, K.A.; Andresen, A.; Stern, R.J.; Manton, W.I.; Omar, S.A.; Maurice, A.E. U-Pb zircon and Sr-Nd-Hf isotopic evidence for a juvenile origin of the El-Shalul Granite, Central Eastern Desert, Egypt. *Geol. Mag.* **2012**, *149*, 783–797. [CrossRef]
95. Zoheir, B.; Goldfarb, R.; Holzheid, A.; Helmy, H.; El Sheikh, A. Geochemical and geochronological characteristics of the Um Rus granite intrusion and associated gold deposit, Eastern Desert, Egypt. *Geosci. Front.* **2019**, *11*, 325–345. [CrossRef]
96. El Bahariya, G.A.; Abu anbar, M.M.; El Galy, M.M. Petrology and geochemistry of Um Rus and Samadi granites, central Eastern Desert, Egypt: Implications for I-type granites of variable magma sources. *Ann. Geol. Surv. Egypt* **2008**, *39*, 1–15.
97. Anderson, P.V.; Kerr, B.J.; Weber, T.E.; Ziemer, C.J.; Shurson, G.C. Determination, and prediction of digestible and metabolizable energy from chemical analysis of corn coproducts fed to finishing pigs. *J. Anim. Sci.* **2012**, *90*, 1242–1254. [CrossRef]
98. Ali, K.A.; Zoheir, B.A.; Stern, R.J.; Andresen, A.; Whitehouse, M.J.; Bishara, W.W. Lu-Hf and O isotopic compositions on single zircons from the Northeastern Desert of Egypt, Arabian- Nubian shield: Implications for crustal evolution. *Gondwana Res.* **2016**, *32*, 181–192. [CrossRef]
99. Bentor, Y.K. The crustal evolution of the Arabo-Nubian massif with special reference to the Sinai Peninsula. *Precambrian Res.* **1985**, *28*, 1–74. [CrossRef]
100. Andresen, A.; El-Rus, M.M.A.; Myhre, P.I.; Boghdady, G.Y.; Corfu, F. U-Pb TIMS age constraints on the evolution of the Neoproterozoic Meatiq Gneiss Dome, Eastern Desert, Egypt. *Int. J. Earth Sci.* **2009**, *98*, 481–497. [CrossRef]
101. Andresen, A.; Abu El-Enen, M.M.; Stern, R.J.; Wilde, S.A.; Ali, K.A. The Wadi Zaghra metaconglomerates of Sinai, Egypt: New constraints on the Ediacaran tectonic evolution of the northernmost Arabian-Nubian Shield. *Int. Geol. Rev.* **2014**, *56*, 1020–1038. [CrossRef]
102. Morag, N.; Avigada, D.; Gerdesb, A.; Belousovac, E.; Harlavand, Y. Crustal evolution and recycling in the northern Arabian-Nubian Shield: New perspectives from zircon Lu–Hf and U-Pb systematics. *Precambrian Res.* **2011**, *186*, 101–116. [CrossRef]
103. El-Manharawy, S.M. Geochronological Investigations of Some Basement Rocks in the Central Eastern Desert, Egypt, between Latitudes 25"-26" N. Ph.D. Thesis, Cairo University, Cairo, Egypt, 1977; 220p.
104. Eliwa, H.A.; Breitkreuz, C.; Murata, M.; Khalaf, I.M.; Bühler, B.; Itaya, T.; Takahashi, T.; Hirahara, Y.; Miyazaki, T.; Kimura, J.I.; et al. SIMS zircon U-Pb and mica K–Ar geochronology, and Sr-Nd isotope geochemistry of Neoproterozoic granitoids and their bearing on the evolution of the northeastern Desert, Egypt. *Gondwana Res.* **2014**, *25*, 1570–1598. [CrossRef]
105. Johnson, P.R.; Andresen, A.; Collins, A.S.; Fowler, A.R.; Fritz, H.; Ghebreab, W.; Kusky, T.; Stern, R.J. Late Cryoge-nian-Ediacaran history of the Arabian-Nubian Shield: A review of depositional, plutonic, structural, and tectonic events in the closing stages of the northern East African Orogen. *J. Afr. Earth Sci.* **2011**, *61*, 167–232. [CrossRef]
106. Moghazi, A.M.; Harbi, H.M.; Ali, K.A. Geochemistry of the Late Neoproterozoic Hadb adh Dayheen ring complex, Central Arabian Shield: Implications for the origin of rare-metal-bearing post-orogenic A-type granites. *J. Asian Earth Sci.* **2011**, *42*, 1324–1340. [CrossRef]
107. Gahlan, H.A.; Azer, M.K.; Al-Hashim, M.H.; Heikal, M.T.S. Highly evolved rare-metal bearing granite overprinted by alkali metasomatism in the Arabian Shield: A case study from the Jabal Tawlah granites. *J. Afr. Earth Sci.* **2022**, *192*, 104556. [CrossRef]

108. Yang, W.-B.; Niu, H.-C.; Hollings, P.; Zurevinski, S.E.; Bo Li, N. The role of recycled oceanic crust in the generation of alkaline A-type granites. *J. Geophys. Res. Solid Earth* **2017**, *122*, 7975–7983. [CrossRef]
109. Mushkin, A.; Navon, O.; Halicz, L.; Hartmann, G.; Stein, M. The petrogenesis of A-type magmas from the Amram Massif, southern Israel. *J. Petrol.* **2003**, *44*, 815–832. [CrossRef]
110. Kessel, R.; Stein, M.; Navon, O. Petrogenesis of late Neoproterozoic dikes in the northern Arabian-Nubian Shield Implication for the origin of A-type granites. *Precambrian Res.* **1998**, *92*, 195–213. [CrossRef]
111. Weissman, A.; Kessel, R.; Oded, N.; Mordechai, S. The petrogenesis of calc-alkaline granites from the Elat massif, Northern Arabian–Nubian shield. *Precambrian Res.* **2013**, *236*, 252–264. [CrossRef]
112. Tindle, A.G.; Webb, P.C. Estimation of lithium contents in trioctahedral micas using microprobe data: Application to micas from granitic rocks. *Eur. J. Mineral.* **1990**, *2*, 595–610. [CrossRef]